ELSEVIER

PII: S0032-3861(96)00703-3

Polymer Vol. 38 No. 8, pp. 1885–1902, 1997

0032-3861/97/$17.00 + 0.00

Evaluation of the fracture behaviour of nylon 6/SEBS-*g*-MA blends

Y. Kayano*, H. Keskkula and D. R. Paul†
Department of Chemical Engineering and Center for Polymer Research, University of Texas at Austin, Austin, TX 78712, USA
(Received 18 April 1996)

High speed fracture behaviour of nylon 6/SEBS-*g*-MA blends with rather small rubber particles near the lower limit for rubber toughening is characterized by the standard Izod impact test and the Vu-Khanh methodology. This characterization expands on previous reports that have examined the standard Izod impact strength of nylon 6 blends with various maleic anhydride grafted styrene-(ethylene-*co*-butylene)-styrene (SEBS-*g*-MA) materials including the ductile–brittle transition behaviour that occurs when the rubber particle size and the test temperature are varied. Load–deflection curves and impact strength of blends with different rubber particle sizes, using both thick and thin specimens, are also reported. Load–deflection curves of tough blends do not show significant differences after normalization by specimen thickness. Morphological features near crack tips formed at high speed were examined by microscopy to gain insight about the sequence of events that occur during crack propagation. All blends examined here show four different regions, i.e. an extensive shear yield zone, a shear yield zone, a cavitation zone and an apparent non-deformed zone within a visible whitened zone. Vu-Khanh parameters, fracture energy at initiation and tearing modulus, show a strong relation to the average rubber particle size and the deformed zone size.

(Keywords: blends; nylon; SEBS)

INTRODUCTION

There has been considerable commercial and scientific interest in the toughening of polyamides with maleated elastomers such as ethylene–propylene based rubber (EPR), or hydrogenated styrene/butadiene triblock copolymers, SEBS[1–12]. During melt processing, the maleic anhydride (MA) grafted to the rubber reacts with the amine end groups on the polyamide chain to form a graft copolymer which allows the rubber, e.g. EPR-*g*-MA or SEBS-*g*-MA, to be dispersed as fine particles in the polyamide matrix and simultaneously strengthens the interface between these phases. The morphology of such blends is a key issue in the degree of toughening achieved and is influenced by a number of factors including the degree of maleation of the rubber, end group content and configuration of the polyamide, rheological characteristics, processing conditions, etc.[8,13–16]. For a fixed rubber content, super-tough blends can be achieved if the rubber particles are within a certain size range[1,6,17–21]. The upper particle size limit, $\approx 1\ \mu$m, is well known in the literature and has been interpreted in terms of a model that considers the interparticle distance as a more fundamental parameter than particle size[3]. The lower particle size limit, $\approx 0.1\ \mu$m, has been determined only more recently, and thus far, the only physical interpretation associated with it has been speculation about the difficulty in cavitation of such small rubber particles[22,23].

Most of the literature in this area has relied on the use of the standard notched Izod impact test or similar procedures to characterize the toughness of these blends. These methods have been used because of convenience and their general use in the plastics industry. They allow easy comparison with other systems; however, the fracture energies obtained by these tests are certainly not material constants and provide only a limited picture of how the material responds to stress in the presence of a crack.

More sophisticated test methods based on fracture mechanics offer means to better characterize the toughness and to understand the deformation mechanisms that occur in toughened engineering thermoplastics[24–40]. However, techniques based on linear elastic fracture mechanics (LEFM) are not fully appropriate for such pseudo-ductile materials. Furthermore, determination of the classical critical stress intensity factor (K_{IC}) requires testing of very thick specimens for materials having low yield strength and high toughness, such as rubber toughened blends, in order to satisfy the small scale yield criterion[41,42]. Such thick specimens cannot be formed easily by injection moulding, which is a preferred method for fabricating plastic parts. For these reasons, the *J*-contour integral method has been recently regarded as more appropriate for such polymeric materials and has the benefit of not requiring exceedingly thick specimens[42,43]. However, the thickness required is still often beyond what can be conveniently injection moulded. Rigorous measurement of J_{IC} involves use of rather specialized equipment and techniques.

A technique recently proposed by Vu-Khanh[33] offers

* Permanent address: Mitsubishi Gas Chemical Co., 6-2 Higasi-Yahata, 5-Chome, Hiratsuka-shi 254, Japan
† To whom correspondence should be addressed

an approach for characterizing fracture that is a useful compromise between rigorous fracture mechanics methodology and the simplicity of Izod or Charpy measurements. In this method, the energy required to fracture a specimen, U, with a ligament area, A, is measured by a standard or instrumented impact tester. It has the advantage of high test speeds corresponding to impact conditions as opposed to essentially static loading conditions usually employed in J_{IC} measurements. The analysis of these types of data, as proposed by Vu-Khanh, yields a fracture energy at initiation, G_i, and a measure of the additional energy associated with propagating the fracture, or tearing modulus, T_a. Vu-Khanh has claimed that the fracture energy at initiation, G_i, is equivalent to the critical J-integral for fracture, J_{IC}. Mai[44] pointed out that the Vu-Khanh approach is equivalent to the essential work analysis proposed by Mai and coworkers and Hodgkinson and Williams[31,45–47] and have questioned equating G_i to J_{IC}. Regardless of the interpretation used, this approach provides considerable useful information about the fracture process that goes well beyond the Izod or Charpy tests, both of which may be regarded as single point methods (one value of A) in this context.

Previous papers have examined the standard Izod impact strength of nylon 6 blends with various SEBS-*g*-MA materials including the ductile–brittle transition behaviour that occurs when the rubber particle size and the test temperature are varied[11,12]. The purpose of this paper is to provide a more in-depth examination of the fracture behaviour of these blends using various toughness evaluation methods and post mortem transmission electron microscopy (TEM) techniques. All of the blends examined here contain very small rubber particles that are near the lower limit for toughening at room temperature.

EXPERIMENTAL

Materials and process conditions

The nylon 6 used in this study is a commercial material from Allied-Signal designated as Capron 8207F; it is a medium molecular weight grade having balanced end groups. Blends of this nylon 6 were made with styrene/ethylene–butylene/styrene triblock copolymers obtained from Shell Chemical Co. SEBS-*g*-MA materials of three different levels of maleation were used; in addition mixtures of an unfunctionalized SEBS with the SEBS-*g*-MA having the highest level of maleation were also used to prepare blends with nylon 6. *Table 1* shows pertinent information on these materials. Compositions of all the blends used in this study are shown in *Table 2*.

Before melt processing, all the materials were predried for 16 h at 80°C in a vacuum oven. Blends were prepared by two extrusion passes through a Killion single screw extruder ($L/D = 30$, $D = 2.54$ cm) at 240°C and 40 rpm to obtain a stable morphology[11]. The blends were injection moulded into Izod bars (ASTM D256) that were either 3.13 mm or 6.25 mm thick (see *Figure 1*) using an Arburg Allrounder injection moulding machine set at a melt temperature of 240°C. Specimens without defects were selected for testing and kept in a dessicator under vacuum to avoid water absorption by the nylon 6 matrix[48,49].

Specimen geometry and Dynatup SN3PB configuration

Figure 1 shows the specimen geometry tested in the single-notch, three-point-bend configuration (SN3PB) using an instrumented Dynatup Drop Tower Model 8200. The guide slit (0.25 mm) was cut by a circular saw and the sharp notch was produced by tapping a fresh razor blade cooled in liquid nitrogen. All tests were made

Table 1 Materials used

Designation used here	Material (commercial designation)	Composition	Molecular weight	Source
Nylon 6	Nylon 6 (Capron 8207F)	End-group content: $[NH_2] = 47.9\ \mu eq\ g^{-1}$; $[COOH] = 43.0\ \mu eq\ g^{-1}$	$\bar{M}_n = 22\,000$[a]	Allied Signal, Inc.
SEBS	Styrene/ethylene-butene/styrene (Kraton G 1652)	29% styrene	Styrene block = 7000 EB block = 37 500	Shell Chemical Co.
SEBS-*g*-MA-2%	Styrene/ethylene-butene/styrene (Kraton FG-1901X)	29% styrene 1.84% MA[b]	–	Shell Chemical Co.
SEBS-*g*-MA-1%	Styrene/ethylene-butene/styrene (Kraton FG-1921X)	29% styrene 0.96% MA[b]	–	Shell Chemical Co.
SEBS-*g*-MA-0.5%	Styrene/ethylene-butene/styrene (Kraton RP-6510)	29% styrene 0.46% MA[b]	–	Shell Chemical Co.

[a] From intrinsic viscosity measurements using $[\eta] = 5.26 \times 10^{-4}\ \bar{M}_w^{0.745}$ assuming $\bar{M}_n = \frac{1}{2}\bar{M}_w$[50]
[b] Determined by elemental analysis after solvent/non-solvent purification

Table 2 Blend compositions

Designation used here	Composition[a]	% MA in rubber phase
Nylon 6	8207F	–
SEBS-*g*-MA-2%	80% 8207F + 20% FG-1901X	1.84
75% SEBS-*g*-MA-2% + 25% SEBS	80% 8207F + 20% (75% FG-1901X + 25% G 1652)	1.38
50% SEBS-*g*-MA-2% + 50% SEBS	80% 8207F + 20% (50% FG-1901X + 50% G 1652)	0.92
25% SEBS-*g*-MA-2% + 75% SEBS	80% 8207F + 20% (25% FG-1901X + 75% G 1652)	0.46
SEBS-*g*-MA-1%	80% 8207F + 20% FG-1921X	0.96
SEBS-*g*-MA-0.5%	80% 8207F + 20% RP 6510	0.46

[a] Commercial designations for the various materials are defined in *Table 1*

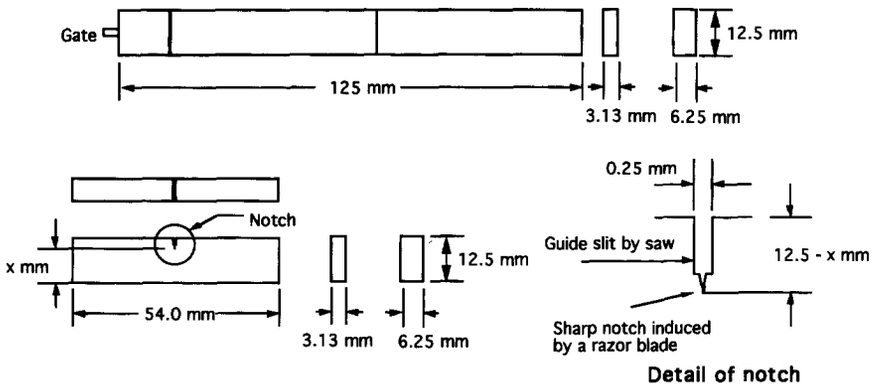

Figure 1 Specimen geometry used in single-notch, three-point-bend, SN3PB, impact testing by Dynatup

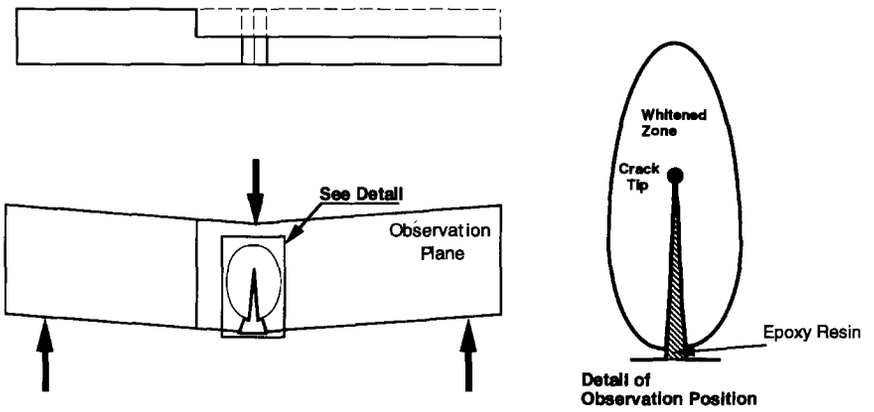

Figure 2 Schematic of arrested crack specimen for TEM observation

by dropping a 10 kg weight at a speed of 3.5 m s^{-1} at the point of contact with the specimen, the same as that specified in the standard Izod test, using a span size of 48 mm. During the test, a load cell in the tup measures the force generated within the deformed specimen. Assuming that the hammer does not change speed significantly during the fracture due to the energy absorbed by the specimen and the effects of gravity, the load–deflection curve can be obtained from the load–time curve. The integral of the load–deflection curve gives the energy absorbed by the specimen during fracture. Load–deflection curves and ductile–brittle transition temperatures were measured using a constant ligament length of 10 mm. In other tests, the ligament length was varied.

TEM observation

TEM was used to observe the morphology of injection moulded blends. Observation planes were chosen parallel to injection flow at the centre and edge of thick specimens (6.25 mm).

TEM was also used to observe the deformation around the tip of arrested cracks. These arrested cracks were generated in 6.25 mm thick specimens with a 10 mm ligament size using the technique shown in *Figure 2*. Crack extension was arrested at the mid-point of the original ligament by adjusting the height of the hammer stoppers. These partially fractured specimens were embedded in epoxy resin (Araldite 502) to avoid further deformation during preparation for microtoming. A block containing the crack was cut from the specimen by a milling machine and a fresh razor blade. The observation plane was selected from the centre of the thickness direction and parallel to both the injection flow and the crack extension directions. After making a mesa-cut, thin sections (15–20 nm) were prepared by a Reichert–Jung Ultracut E microtome under cryogenic conditions (−45°C) with a diamond knife. Thin sections were stained by exposure to the vapours of a ruthenium tetroxide solution (0.5%) for 20 min at room temperature. The rubber particles appear black in the TEM images. Photomicrographs were made sequentially from the crack tip to the undeformed region using a JEOL 200 CX TEM at an accelerating voltage of 120 kV. TEM observations were made under both bright and dark field conditions to obtain a better understanding of where voids had formed.

MORPHOLOGY

Figures 3 and *4* show TEM photomicrographs that characterize the morphology of nylon 6 blends with the various SEBS-*g*-MA-2%/SEBS mixtures and SEBS-*g*-MA-X% materials. The high magnification TEM photomicrograph shown in *Figure 5* reveals the microdomain structure inside the block copolymer particles. The area, a_i, of each rubber particle seen in the field of view of the TEM photomicrograph was determined by the aid of a semi-automatic digital analysis technique based on Image® software from the National Institutes of Health. The weight average particle diameter, $\bar{d}_w$, was calculated from

$$\bar{d}_w = \frac{\sum_{i=1}^{n} n_i d_i^2}{\sum_{i=1}^{n} n_i d_i} \quad (1)$$

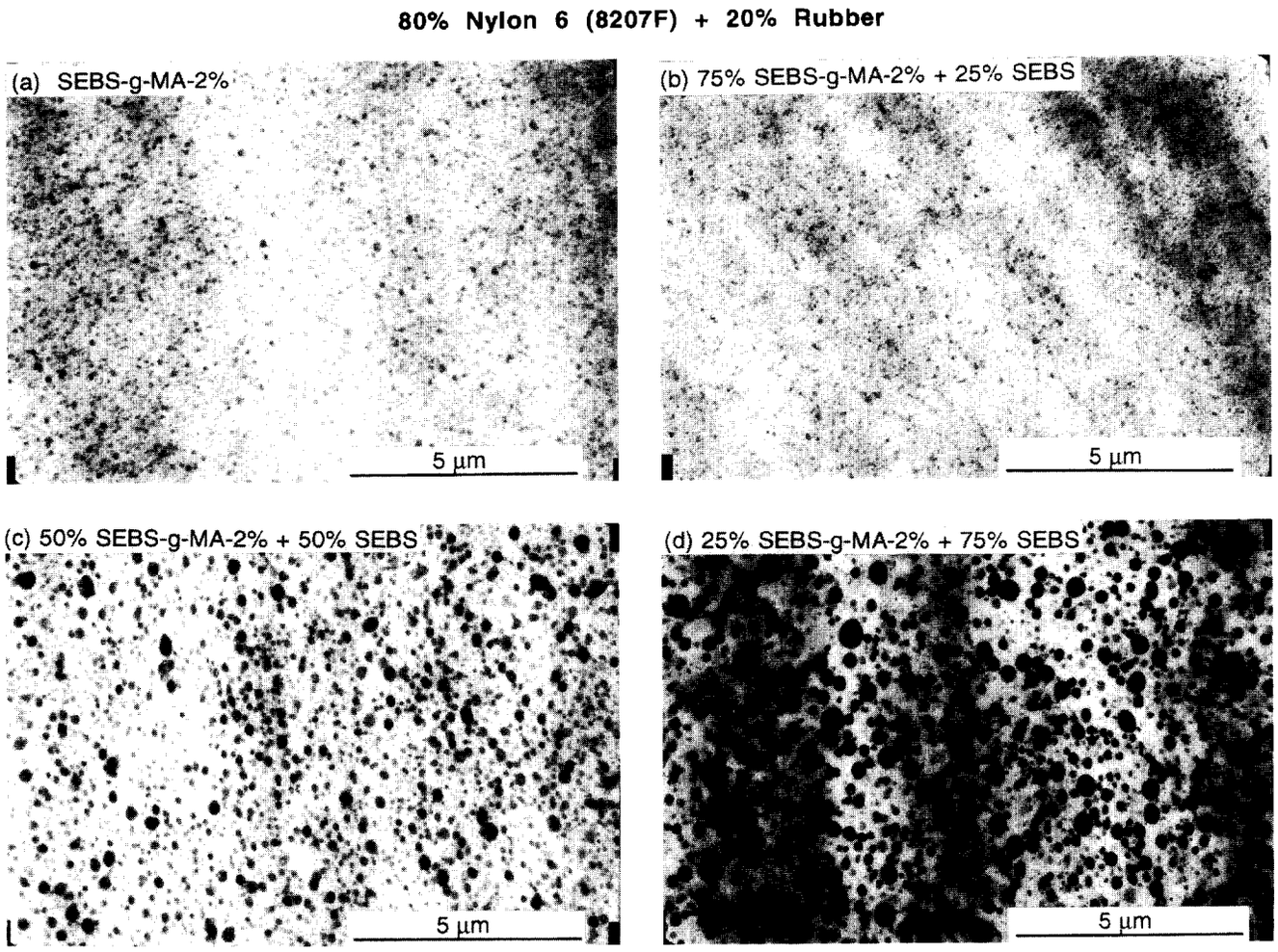

Figure 3 TEM photomicrographs of blends based on SEBS-*g*-MA-2% and SEBS mixtures: (a) 100% SEBS-*g*-MA-2%; (b) 75% SEBS-*g*-MA-2% + 25% SEBS; (c) 50% SEBS-*g*-MA-2% + 50% SEBS; (d) 25% SEBS-*g*-MA-2% + 75% SEBS

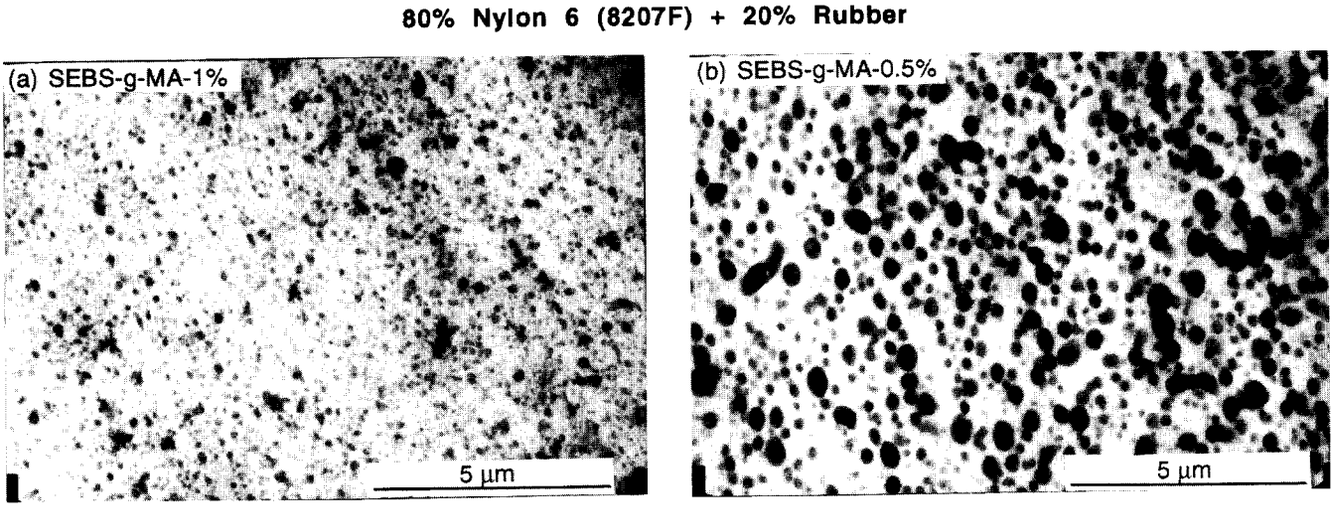

Figure 4 TEM photomicrographs of blends based on SEBS-*g*-MA-X%: (a) SEBS-*g*-MA-1%; (b) SEBS-*g*-MA-0.5%

where n_i is the number of particles having the apparent particle diameter d_i computed from $2\sqrt{a_i/\pi}$. This average is frequently used for showing the relationship between particle size and toughness of such blends. The weight-average particle size found for the various blends are summarized in *Table 3*; the particle size decreases as the MA content of the rubber phase increases[8,11–15,21].

The MA content of the rubber phase was varied by using rubber with different levels of maleation, SEBS-*g*-MA-X% materials and by mixing SEBS-*g*-MA-2% with SEBS in various proportions. When compared at the same levels of MA content, i.e. 25% SEBS-*g*-MA-2%/75% SEBS vs SEBS-*g*-MA-0.5% and 50% SEBS-*g*-MA-2%/50% SEBS vs SEBS-*g*-MA-1%, the blends

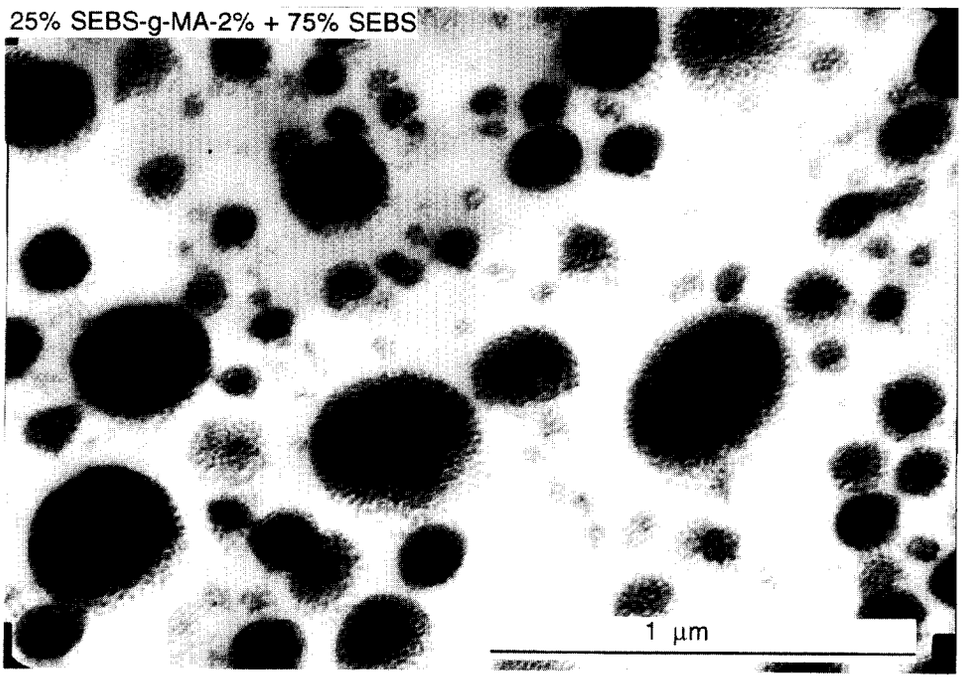

Figure 5 High magnification TEM photomicrographs of a blend based on 25% SEBS-*g*-MA-2% + 75% SEBS mixture

Table 3 Morphology and deformed zone observation of 80% nylon 6 (8207F) + 20% rubber blends

Rubber phase	Weight-average particle diameter, $\bar{d}_w$ (μm)	Deformed zone size from TEM, *a* (μm)	Whitened zone size (mm)		Degree of rubber particle cavitation
			A	B	
SEBS-*g*-MA-2%	0.056	8	< 0.1	< 0.1	Little
75% SEBS-*g*-MA-2% + 25% SEBS	0.097	21	< 0.1	< 0.1	Moderate
50% SEBS-*g*-MA-2% + 50% SEBS	0.136	48	0.5	1.0	Extensive
25% SEBS-*g*-MA-2% + 75% SEBS	0.202	75	0.9	1.9	Extensive
SEBS-*g*-MA-1%	0.161	15	0.1	< 0.1	Extensive
SEBS-*g*-MA-0.5%	0.268	37	0.7	1.7	Extensive

based on the SEBS-*g*-MA-X% materials have slightly larger rubber particles. A previous paper[11] reported an opposite trend based on TEM photomicrographs from injection moulded 3.13 mm bars observed in the direction perpendicular to the flow. The differences in specimen thickness and observation direction used in the two studies may account, at least in part, for this discrepancy.

IZOD AND DYNATUP IMPACT STRENGTH OF THIN SPECIMENS WITH STANDARD NOTCHES

Figure 6 shows the Izod impact strength as a function of testing temperature for the various blends described in *Table 2* plus neat nylon 6 measured using thin (3.13 mm) specimens with standard notches. *Figure 7* shows the corresponding data determined by the Dynatup testing machine for the same materials and specimen geometry. Each rubber toughened material shows a loss of toughness by both tests as the test temperature is lowered. Some blends show a decrease and then an increase in impact strength as the temperature is raised above the ductile–brittle transition; this behaviour will be explored in more detail in subsequent papers[50–52]. Values of impact strength at room temperature and the ductile–brittle transition temperature for each blend determined by the two methods are summarized in *Table 4*. The nylon 6 blend with 25% SEBS-*g*-MA-2%/75% SEBS shows the maximum impact strength at room temperature, using both test methods, of all materials examined here.

Figure 8a shows both the Izod and the Dynatup impact strengths as a function of weight-average rubber particle diameter in the various blends. Blends with smaller rubber particles show lower impact strength at room temperature regardless of the test method used. These blends have rather small rubber particles near the lower limit for toughening[22,23], which explains the decrease in toughness as the rubber particles become smaller. Blends with rubber particles near the upper limit for toughening would show the reverse of this trend. The Izod impact strength for all blends tends to be less than that measured by the Dynatup. The Izod values are approximately 60% of the Dynatup values; see *Figure 8b* where the ratio of the two room temperature measurements are plotted vs Dynatup impact strength. Differences in the sample configuration of the Izod test (cantilever bending) vs that used in the Dynatup (three point bending) are responsible for the inequality of the two measures of impact strength. The fracture mode in Izod impact testing of very ductile materials usually leads to partial breaks that leave a rather large unbroken

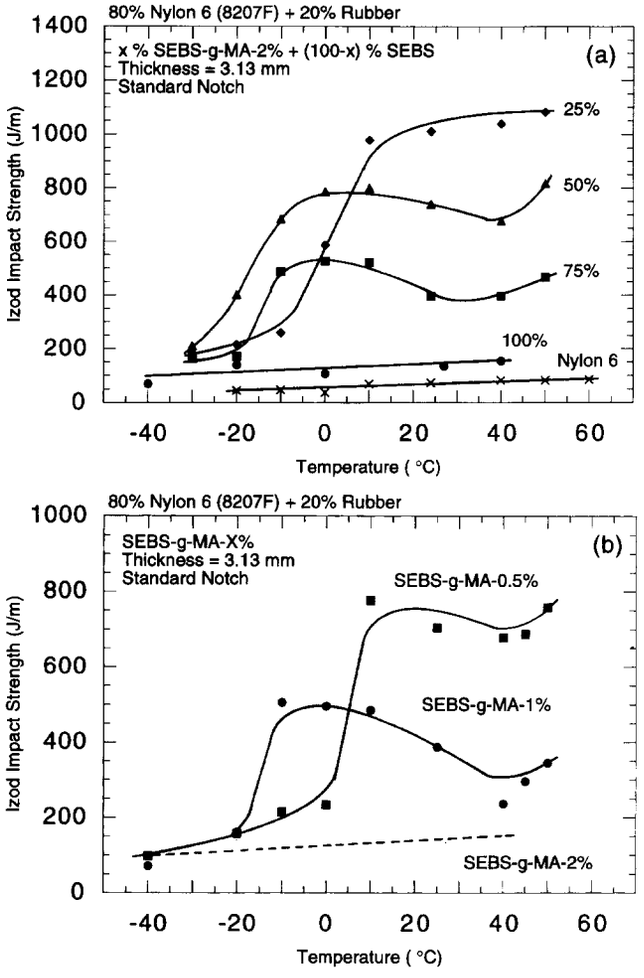

Figure 6 Notched Izod impact strength as a function of temperature for: (a) blends based on SEBS-*g*-MA-2% and SEBS mixtures; (b) blends based on SEBS-*g*-MA-X%

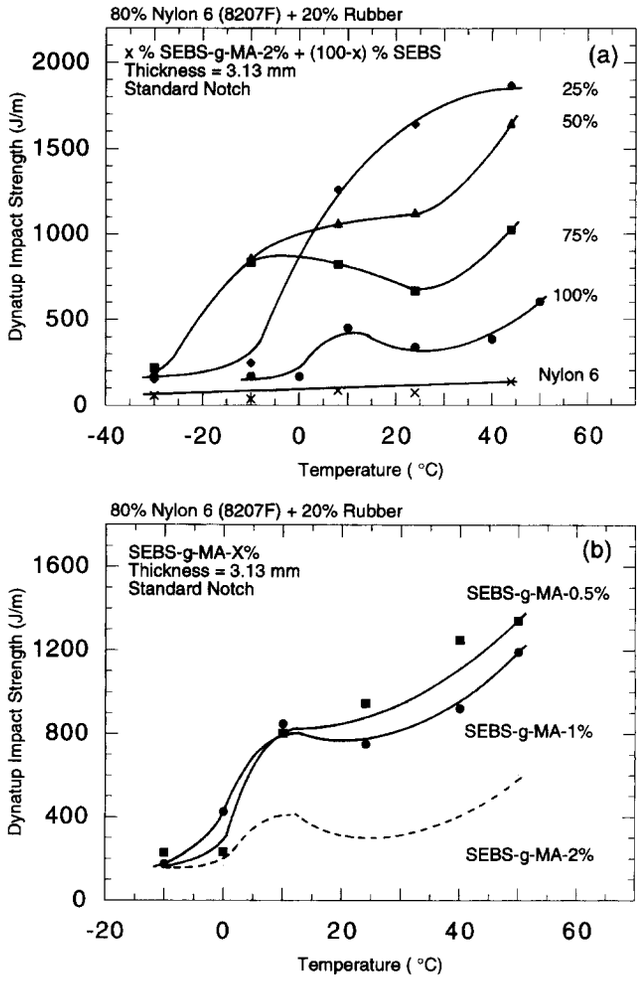

Figure 7 Dynatup impact strength as a function of temperature for: (a) blends based on SEBS-*g*-MA-2% and SEBS mixtures; (b) blends based on SEBS-*g*-MA-X%

Table 4 Summary of impact strength characterization[a]

	Izod impact ($J\,m^{-1}$)	Dynatup impact strength[b] ($J\,m^{-1}$)				Vu-Khanh parameters G_i ($kJ\,m^{-2}$), T_a ($10^6\,kJ\,m^{-4}$)							
	3.13 mm	3.13 mm		6.25 mm		3.13 mm		6.25 mm					
						24°C		15°C		24°C		40°C	
80% Nylon (8207F) + 20% Rubber	Standard notch	Standard notch	Sharp notch	Standard notch	Sharp notch	G_i	T_a	G_i	T_a	G_i	T_a	G_i	T_a
SEBS-*g*-MA-2%	135	339 (+5)	324 (+5)	169 (+15)	133 (+22)	16.1	0.0	14.4	0.0	16.2	0.0	15.2	0.0
75% SEBS-*g*-MA-2% + 25% SEBS	398 (−15)	669 (−25)	644 (0)	309 (+15)	288 (+15)	15.0	3.0	25.3	0.0	28.0	0.0	20.0	0.0
50% SEBS-*g*-MA-2% + 50% SEBS	740 (−20)	1126 (−15)	1142 (−15)	880 (0)	864 (0)	27.8	6.8	24.8	1.8	32.6	2.0	22.0	2.2
25% SEBS-*g*-MA-2% + 75% SEBS	1012 (0)	1644 (0)	1295 (0)	1443 (0)	1315 (0)	32.2	8.4	32.5	2.6	45.7	3.8	45.7	4.4
SEBS-*g*-MA-1%	388 (−15)	751 (0)	803 (0)	371 (+20)	304 (+10)	9.5	2.6	15.8	0.7	18.4	0.6	24.4	0.1
SEBS-*g*-MA-0.5%	704 (+5)	946 (+5)	1050 (+5)	839 (+12)	779 (+12)	32.7	3.8	29.9	1.5	32.1	1.8	26.5	2.3
Nylon 6	73	72	23	91	30	3.4	0.0	3.2	0.0	3.4	0.0	3.5	0.0

[a] Value in parentheses is the ductile–brittle transition temperature defined as the mid-point of the temperature range over which this change in fracture mode occurs

[b] Tested by Dynatup SN3PB at 24°C

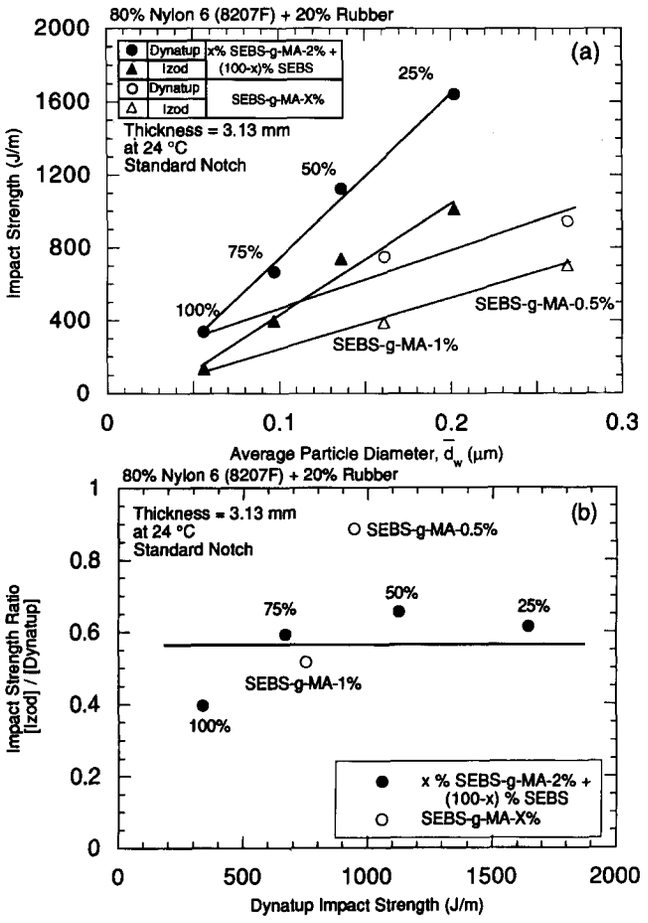

Figure 8 Impact strength by various test methods as a function of an average rubber particle diameter (a), and ratio of Izod to Dynatup impact strengths (b)

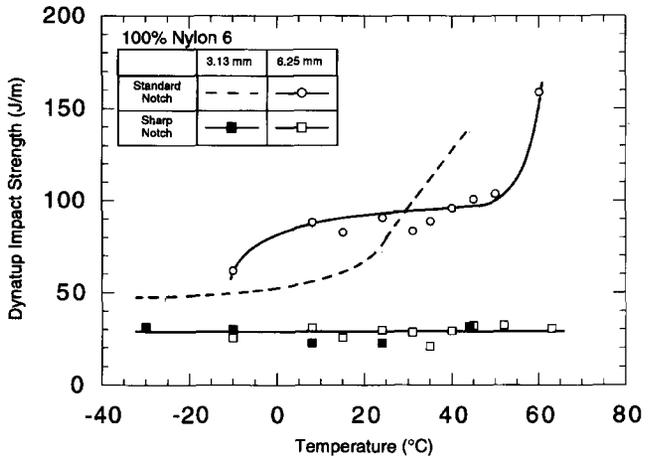

Figure 9 Dynatup impact strength as a function of temperature for Nylon 6

ligament because the specimen deflects out of the path of the hammer. In the Dynatup test used here, the breaks are more likely to be complete, but when hinged breaks do occur there is very little unbroken ligament since it is more difficult for the specimen to deflect out of the path of the hammer in three point bending. Generally, the ductile–brittle transition temperatures obtained using thin specimens with standard notches are about the same from the Dynatup and Izod tests (see *Table 4*). However, for a blend with SEBS-*g*-MA-1%, the difference is 15°C, and the Izod test gives the lower value.

DYNATUP IMPACT TOUGHNESS AS A FUNCTION OF TEMPERATURE

The Dynatup impact strengths for thin and thick specimens of neat nylon 6 with standard and sharp notches are shown in *Figure 9* as a function of temperature. The fracture mode of neat nylon 6 is totally brittle at all testing temperatures shown regardless of specimen geometry. Specimens with standard notches require more energy to break than those with sharp notches because of the greater energy needed for crack initiation from a blunt notch; this reflects the well-known notch sensitivity of polyamide materials[53]. For a given notch geometry, specimen thickness has little influence on the impact strength of nylon 6.

Examples of Dynatup impact strength vs temperature are shown in *Figure 10* for blends of nylon 6 with two SEBS-*g*-MA-2%/SEBS compositions for two specimen thicknesses and notch geometries. The blend of nylon 6 with 100% SEBS-*g*-MA-2%, shown in *Figure 10a*, is not very tough, but it shows rather different behaviour than neat nylon 6. The Dynatup impact strength of this blend is more dependent on specimen thickness than notch geometry. On the other hand, the blend of nylon 6 with 25% SEBS-*g*-MA-2% + 75% SEBS, which is very tough above the ductile–brittle transition temperature, does not show any significant dependency on specimen thickness or notch geometry in the temperature range tested (see *Figure 10b*). Blends of nylon 6 with the two

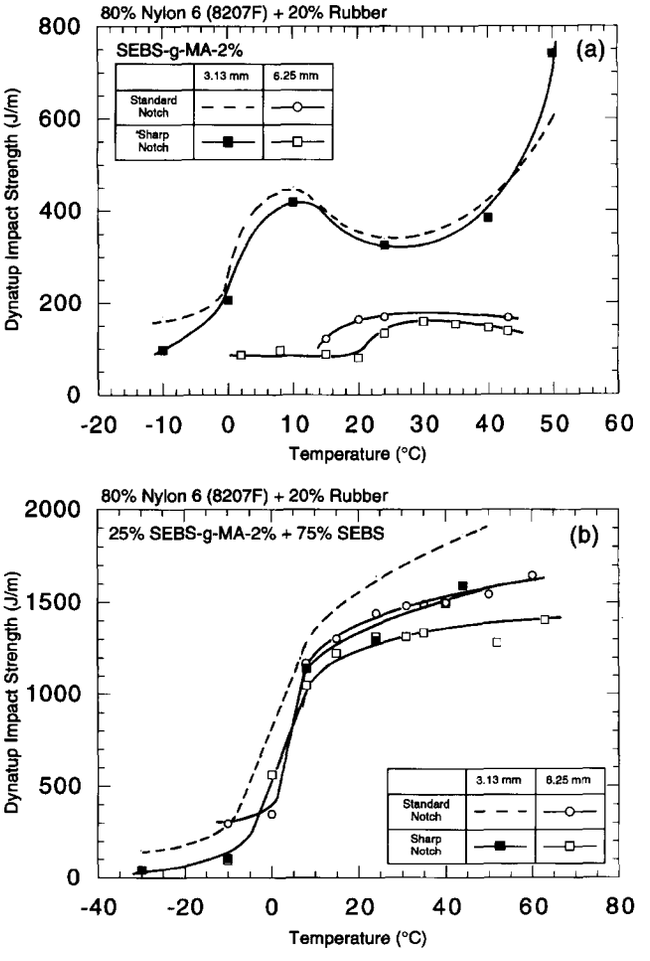

Figure 10 Dynatup impact strength as a function of temperature for the blends based on: (a) SEBS-*g*-MA-2%; (b) 25% SEBS-*g*-MA-2% and 75% SEBS mixture

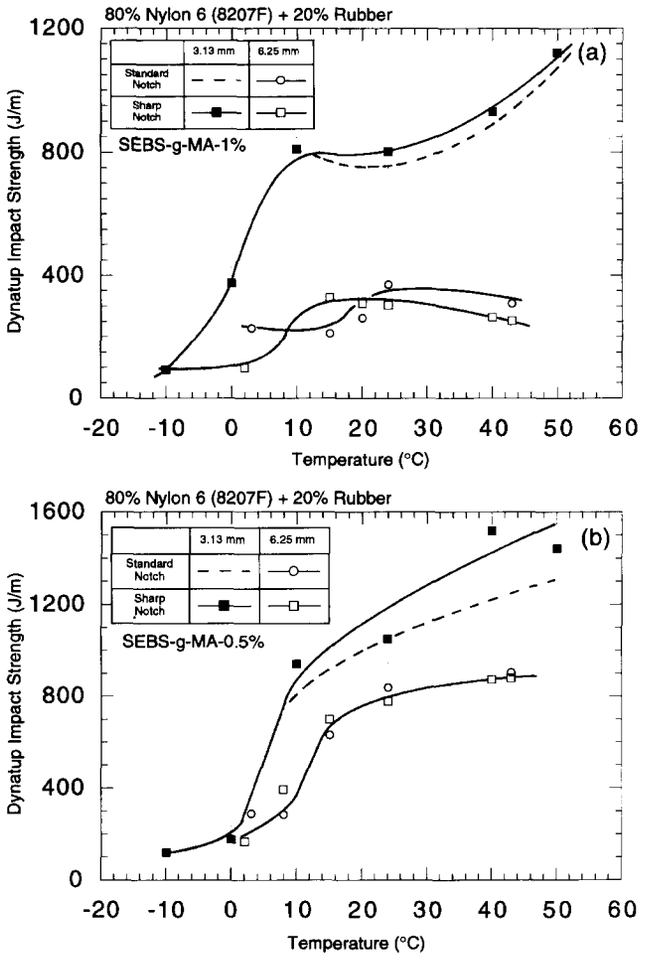

Figure 11 Dynatup impact strength as a function of temperature for the blends based on: (a) SEBS-*g*-MA-1%; (b) SEBS-*g*-MA-0.5%

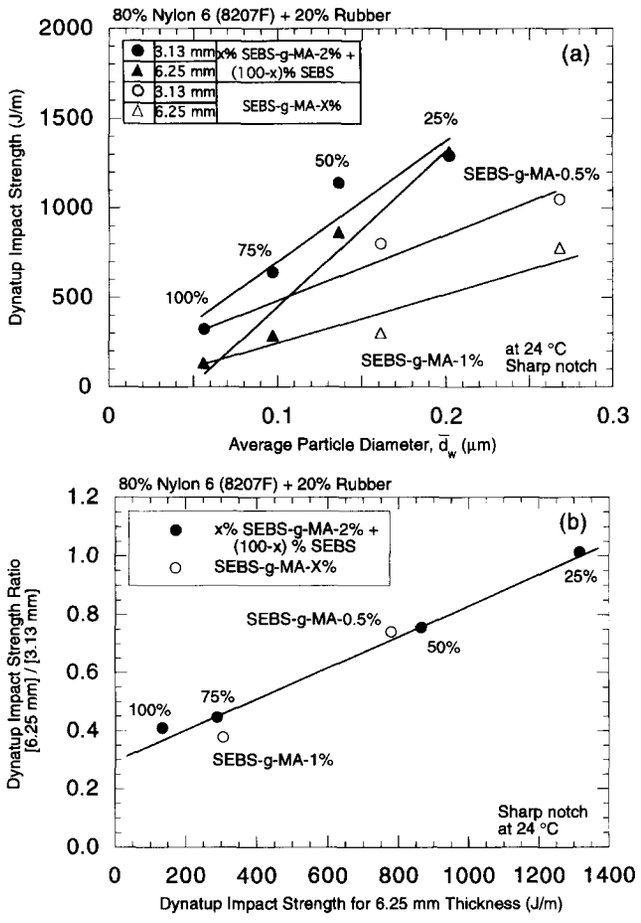

Figure 12 Dynatup impact strength for thin and thick specimens with sharp notches as a function of an average rubber particle diameter (a) and impact strength ratio for thick and thin specimens (b)

SEBS-*g*-MA-X% materials with X = 0.5 and 1% are considerably tougher (see *Figure 11*) than the blend with the maleated rubber with X = 2% (*Figure 10a*), owing to the larger rubber particles formed when the rubber contains a lower amount of MA[11]. The nylon 6/SEBS-*g*-MA-0.5% blend (*Figure 11b*) reaches the highest levels of toughness and has less dependency on specimen geometry than the less tough nylon 6/SEBS-*g*-MA-1.0% blend (*Figure 11a*). The toughness of both materials are relatively insensitive to notch geometry at a given temperature. The results for all blends are summarized in *Figures 12* and *13* and *Table 4*. Dynatup impact strength values for thick (6.25 mm) and thin (3.13 mm) specimens with a sharp notch are shown as a function of the weight-average rubber particle diameter in *Figure 12a*. The Dynatup impact strength for nylon 6/(SEBS-*g*-MA-2%/SEBS) blends for both thin and thick specimens increases linearly with rubber particle size over this range (*Figure 12a*). Blends of nylon 6 with the SEBS-*g*-MA-X% materials also show an increase in room temperature toughness with increasing $\bar{d}_w$; however, at the same values of $\bar{d}_w$, the absolute levels of toughness are lower when X = 0.5 and 1%. Note that the blend of nylon 6 with 10% SEBS-*g*-MA-2% in the rubber phase may be considered as a member of both series in *Figure 12a*. Blends based on SEBS-*g*-MA-X% materials have a relatively narrow distribution of rubber particles sizes (see *Figure 4*) while blends based on SEBS-*g*-MA-2%/SEBS mixtures tend to have a more broad distribution including many smaller particles between large particles. Thus, the interparticle distances for the blends based on SEBS-*g*-MA-2%/SEBS mixtures are smaller than in the blends based on SEBS-*g*-MA-X% materials. This morphological difference may be the cause of the higher impact strength of blends based on the SEBS-*g*-MA-2%/SEBS mixtures. The ratio of the room temperature impact strength for thick relative to thin specimens is shown as a function of impact strength for the thick specimens in *Figure 12b*. The impact strength ratio increases linearly with the absolute toughness of the blend, i.e. tougher blends show less dependence on specimen thickness. Trends similar to those in *Figure 12* for specimens with sharp notches are shown in *Figure 13* for specimens with standard notches. Ductile–brittle transition temperatures obtained by the Dynatup test using specimens with standard and sharp notches are very similar for most of these blends as seen in *Table 4*.

IMPACT LOAD CURVE ANALYSIS

The impact load–deflection curves shown in *Figures 14–16* were signal-conditioned using a digital low pass filter to reduce high frequency vibration components, i.e. 'ringing', received by the load cell as explained previously[54]. *Figure 14* compares impact load–deflection curves measured at room temperature using thick (6.15 mm) specimens with sharp notches for blends of nylon 6 with various SEBS-*g*-MA-2%/SEBS mixtures (plus neat nylon 6). There is no significant difference in

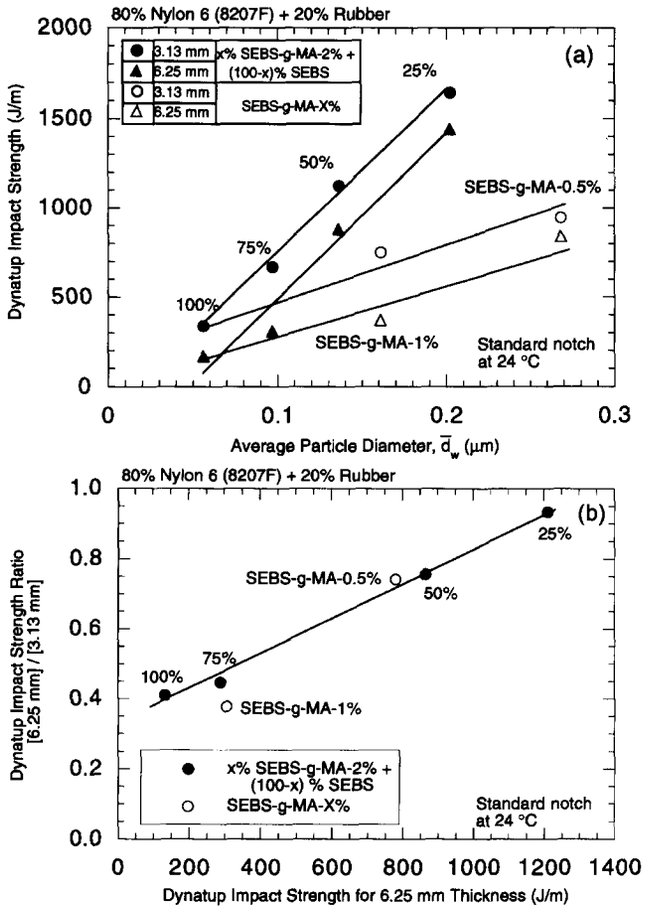

Figure 13 Dynatup impact strength for thin and thick specimens with standard notches as a function of average rubber particle diameter (a) and impact strength ratio for thick and thin specimens (b)

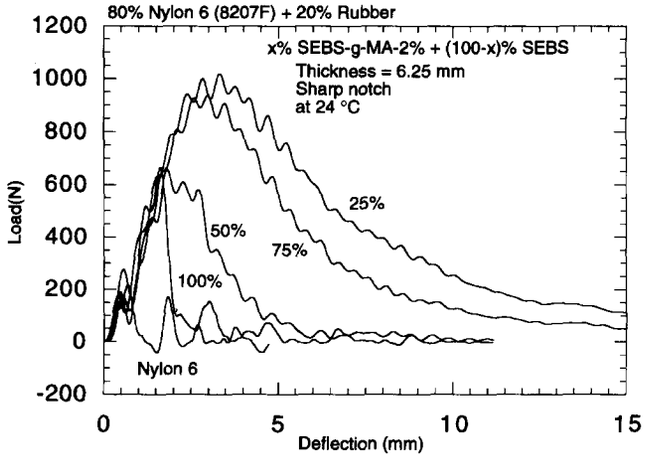

Figure 14 Load–deflection curves obtained by Dynatup at 24°C for thick specimens with sharp notches of the blends based on SEBS-*g*-MA-2% and SEBS mixtures

the initial slopes of the load curves, since all of these materials have about the same tensile modulus[40]. Blends based on lower amounts of the maleated SEBS-*g*-MA materials, which have larger rubber particles, show higher maximum load and larger deflection prior to total fracture. The larger rubber particles in this range increase both the resistance to crack initiation and the energy required to propagate the crack.

Figure 15 shows impact load–deflection curves normalized by specimen thickness for various nylon 6/(SEBS-*g*-MA-2%/SEBS) blends measured at room temperature using thin (3.13 mm) and thick (6.25 mm) specimens with sharp notches. The curves for the blend based on 100% SEBS-*g*-MA-2% are shown in *Figure 15a*. The thin specimens fracture in a ductile manner while the thick specimens show brittle fracture because of the differences in stress state; the thick specimen has a greater tendency for a plane strain condition, and this state of triaxial stress makes matrix yielding more difficult[42,55]. *Figure 15* shows that as the amount of SEBS-*g*-MA-2% in the rubber phase is reduced, which leads to larger rubber particles, there is less sensitivity to specimen thickness in the fracture response over the thickness range tested here. The blend based on 25% SEBS-*g*-MA-2% + 75% SEBS shows exactly the same normalized load curves for both specimen thicknesses (*Figure 15d*). Thus, the impact strength values of these very tough blends are the same regardless of thickness, as shown in *Figures 10b* and *12b*.

Figure 16 shows impact load–deflection curves for nylon 6/25% SEBS-*g*-MA-2%/75% SEBS) blends tested at 15, 24 and 45°C. As the testing temperature increases over this range, these blends show higher loads at the point of initiation and crack extension. This is in accord with the trend of increasing impact strength with temperature above the ductile–brittle transition seen in *Figure 10b* for these materials.

VU-KHANH FRACTURE ANALYSIS

As mentioned earlier, considerably greater insight about the fracture toughness of ductile plastics can be gained from analysis of the fracture energy as a function of the ligament area[24,33,54]. Vu-Khanh showed that the fracture energy per unit of ligament area, U/A, is a linear function of the ligament area A, and defined the two parameters in the relationship

$$\frac{U}{A} = G_i + \frac{1}{2} T_a A \qquad (2)$$

The quantity G_i has been termed the fracture energy at initiation, while T_a has been interpreted as the tearing modulus. Vu-Khanh showed evidence that the fracture energies at initiation, G_i, obtained by this method at low strain rate for toughened nylon 6,6 and a polycarbonate/polyethylene blend are similar in magnitude to the J_{IC} values obtained by other techniques for these methods. Recently Crouch and Huang have also shown that the resistance curve (J–R curve) has a low dependence on testing rate[27]. The two Vu-Khanh parameters can be useful for characterizing the toughness of ductile materials, even though there is some controversy about their physical meaning[44]. An analysis of Dynatup fracture energy using equation (2) was made at various temperatures for the blends described above.

Figure 17 shows the fracture energy per unit area as a function of ligament area for each blend based on various SEBS-*g*-MA-2%/SEBS mixtures obtained at 15, 24 and 40°C using thick (6.25 mm) specimens with sharp notches. All rubber toughened blends have significantly higher values of the fracture energy at initiation, G_i than neat nylon 6 at the test temperatures used. Neat nylon 6 and blends based on SEBS-*g*-MA-2% material and 75% SEBS-*g*-MA-2% + 25% SEBS mixtures have zero values for the tearing modulus, T_a, indicative of their brittle nature. On the other hand, blends based on 50% SEBS-*g*-MA-2% + 50% SEBS mixture and 25%

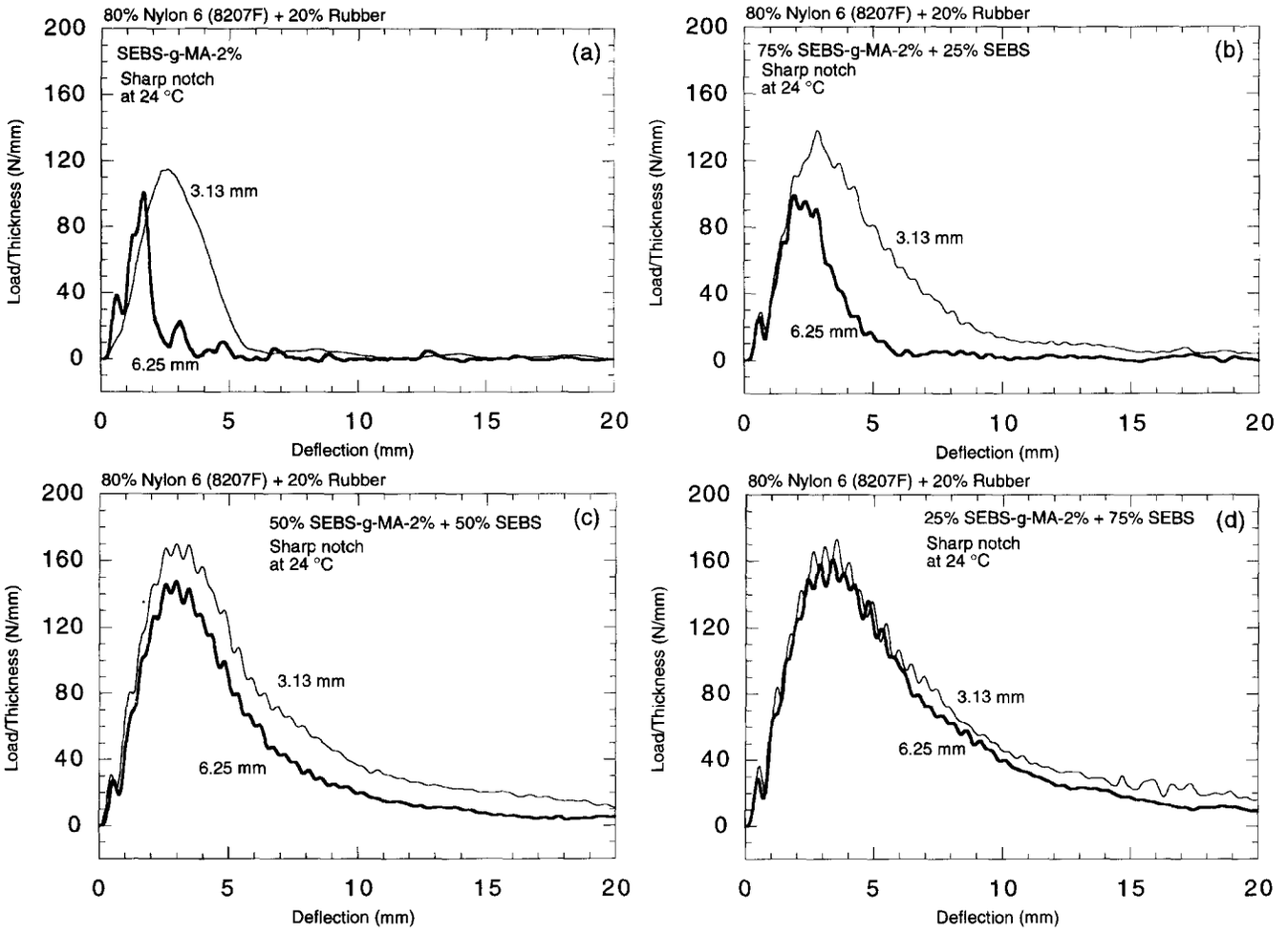

Figure 15 Load–deflection curves obtained by Dynatup at 24°C for thick and thin specimens with sharp notches of the blends based on: (a) 100% SEBS-*g*-MA-2%; (b) 75% SEBS-*g*-MA-2% and 25% SEBS; (c) 50% SEBS-*g*-MA-2% and 50% SEBS; (d) 25% SEBS-*g*-MA-2% and 75% SEBS

SEBS-*g*-MA-2% + 75% SEBS mixture have finite values of T_a reflecting ductile fracture processes.

Figure 18 shows a similar plot for the blends based on SEBS-*g*-MA-2%/SEBS mixtures obtained at 24°C but using thin (3.13 mm) specimens with sharp notches. The slope or tearing modulus for neat nylon 6 and the blend based on pure SEBS-*g*-MA-2% in the rubber phase are zero while all other blends have finite values. The blend based on the 75% SEBS-*g*-MA-2% + 25% SEBS mixture is the only material in this set which shows a significant difference in fracture mode between thin (3.13 mm) and thick (6.25 mm) specimens. *Figure 19* shows the fracture energy per unit area as a function of ligament area for nylon 6/SEBS-*g*-MA-X% blends tested at room temperature using thick (*Figure 19a*) and thin (*Figure 19b*) specimens with sharp notches.

Values of the fracture energy at initiation G_i and the tearing modulus T_a for all specimens are summarized in *Table 4*; *Figure 20* shows these quantities plotted vs rubber particle size for the blends based on SEBS-*g*-MA-2%/SEBS mixtures. Generally, the fracture energy at initiation and the tearing modulus of these blends continuously increase as the rubber particles become larger, i.e. the less SEBS-*g*-MA-2% in the rubber phase. The fracture energy at initiation is about the same when thin and thick specimens are used (see *Figure 20a*). This suggests that a true plane strain condition is approximated when the fracture energy per unit is extrapolated to zero ligament area for both specimen thickness. This is reasonable since this is actually an extrapolation to zero ligament length; thus, the specimen thickness/ligament length ratio goes to infinity in this limit regardless of the sample thickness ensuring a plain strain condition. On this basis, G_i might be a true material parameter independent of specimen geometry. However, the tearing modulus decreases as specimen thickness increases, as seen in *Figure 20b* and *Table 4*. Thus, this parameter clearly is not a true material parameter; more will be said about this later. For these blends, there is a critical rubber particle size below which T_a is zero; this is about 0.1 μm for the thick specimens and 0.05 μm for the thin specimens. The tearing moduli obtained using thin specimens are substantially higher than those obtained using specimens twice as thick. As will be seen later, thin specimens produce larger shear yield zones than do thick specimens, and it is believed that this is in part the cause for the higher values of tearing modulus observed.

Over the limited range used in these experiments, it is difficult to discern a clear trend of how test temperature, above the ductile–brittle transition, affects G_i (see *Figure 20a*). In most cases, T_a increases slightly with temperature over this limited range (see *Figure 20b*).

The benefit of this detailed analysis of fracture in comparison to Izod or Charpy type testing is to differentiate to what extent the increase in energy to produce a complete fracture stems from changes in the fracture energy at initiation, G_i and/or the tearing modulus, T_a. For super-tough materials, it appears that

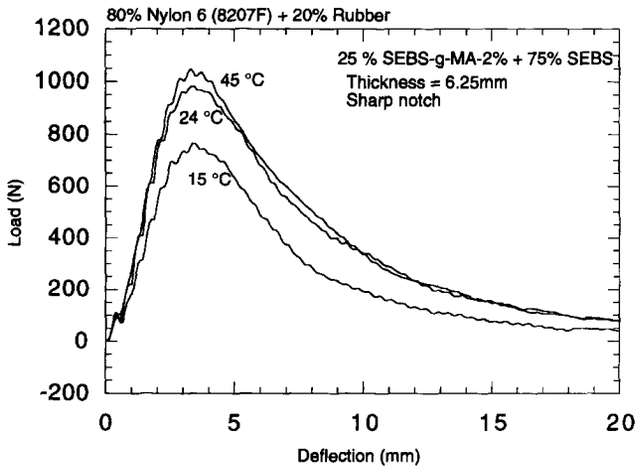

Figure 16 Load–deflection curves obtained by Dynatup at various temperatures for thick specimens with sharp notches of the blends based on 25% SEBS-*g*-MA-2% and 75% SEBS mixture

the Izod impact test emphasizes the tearing modulus since its contribution to the total fracture energy, above the ductile–brittle transition temperature, is much more than that from the fracture energy at initiation; below ductile–brittle temperature, the tearing modulus is essentially zero. It is suggested that the ductile–brittle transition primarily represents the temperature above which the tearing modulus becomes finite. Similarly, as the rubber particle size decreases below the lower limit for toughening at room temperature, the tearing modulus approaches zero. It will be useful to determine whether the parameters G_i and T_a can be related to specific performance requirements of materials.

The Vu-Khanh approach assumes that fracture energy, U, is a function only of the ligament area, A (the product of ligament length, x, and specimen thickness, w), without giving explicit consideration to the fact that the nature of the stress state and the mode of fracture may be affected by the value of x or w individually. As seen above, the value of G_i seems to be independent of specimen thickness, but clearly T_a decreases as the specimen becomes thicker for the materials considered here. For a given ligament length, the fracture energy per unit thickness can be nearly independent of specimen thickness (see for example *Figure 15d*) for some materials. This would correspond to the Izod impact energy being independent of specimen thickness, i.e.

$$\frac{U_1}{w_1} = \frac{U_2}{w_2} \text{ for } w_1 \neq w_2 \tag{3}$$

Inserting this equality into the Vu-Khanh model, equation (2), leads to the following conclusion

$$(T_a)_1 w_1 = (T_a)_2 w_2 \tag{4}$$

if we assume $(G_i)_1 = (G_i)_2$ as suggested earlier. Thus, we see that if T_a were truly a material constant then the Izod impact strength could not be independent of thickness or that if for some material the Izod impact strength is independent of thickness, then T_a is thickness dependent as given by equation (4). In general, it appears that the Vu-Khanh model does a good job of describing how fracture energy depends on ligament length at a fixed specimen thickness which is how ligament area, A, is varied in most experiments. It appears that care should

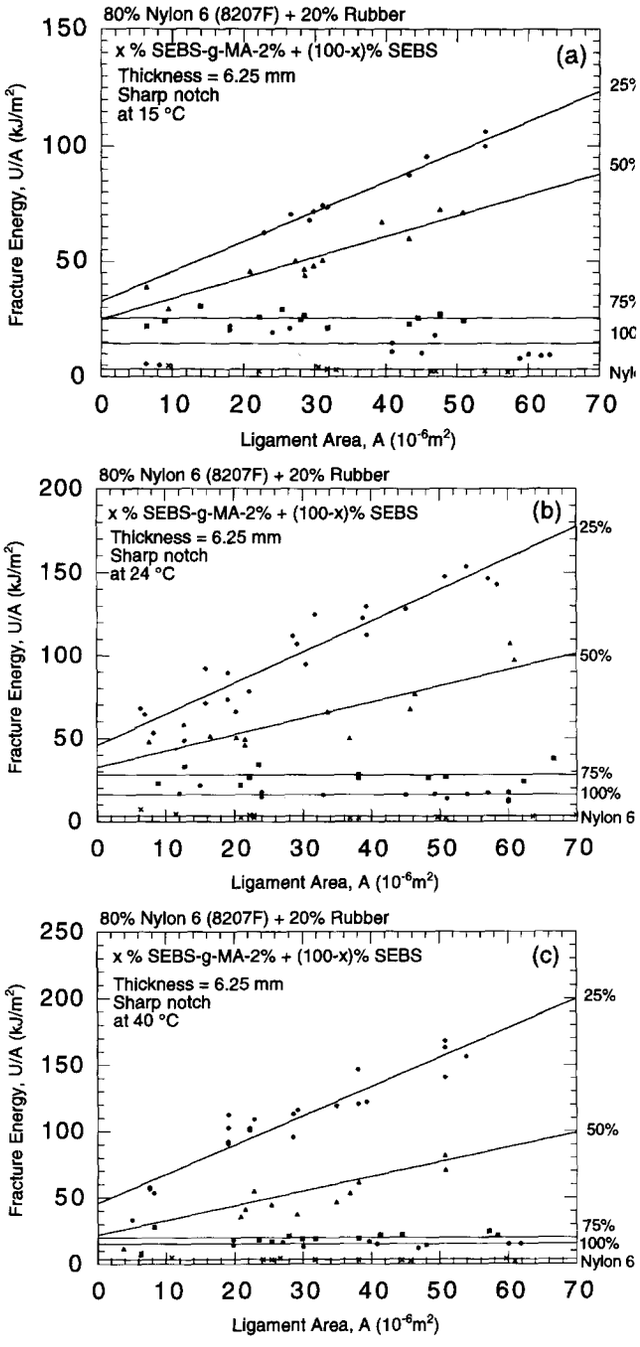

Figure 17 Fracture energy as a function of ligament area for thick specimens with sharp notches of the blends based on SEBS-*g*-MA-2% and SEBS mixtures at: (a) 15°C; (b) 24°C; (c) 40°C

be exercised when using data obtained at one thickness to infer fracture behaviour at another thickness, especially for the term involving the tearing modulus. The literature[55] suggests that the tearing modulus is related to the way the J integral depends on ligament length, viz

$$T_a = \frac{E}{\sigma_y^2} \frac{dJ}{dx} \tag{5}$$

where E is the tensile modulus and σ_y is the yield stress. It would be interesting to compare values computed from equation (5) with those obtained by the Vu-Khanh type analysis, and to better understand the influence of specimen thickness in both the J integral measurement and in the Vu-Khanh type experiment.

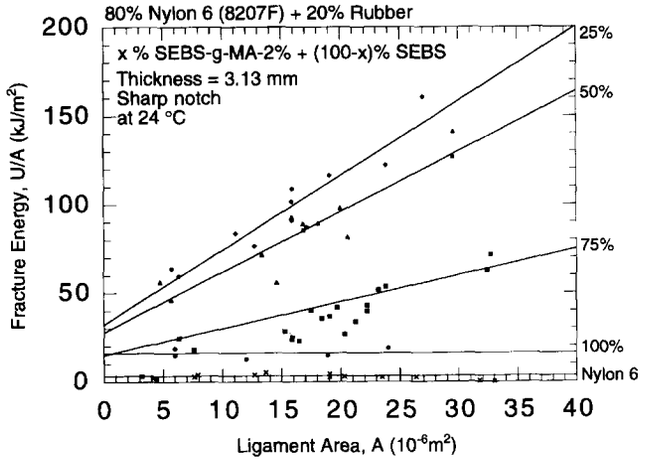

Figure 18 Fracture energy as a function of ligament area for thin specimens with sharp notches of the blends based on SEBS-*g*-MA-2% and SEBS mixtures at 24°C

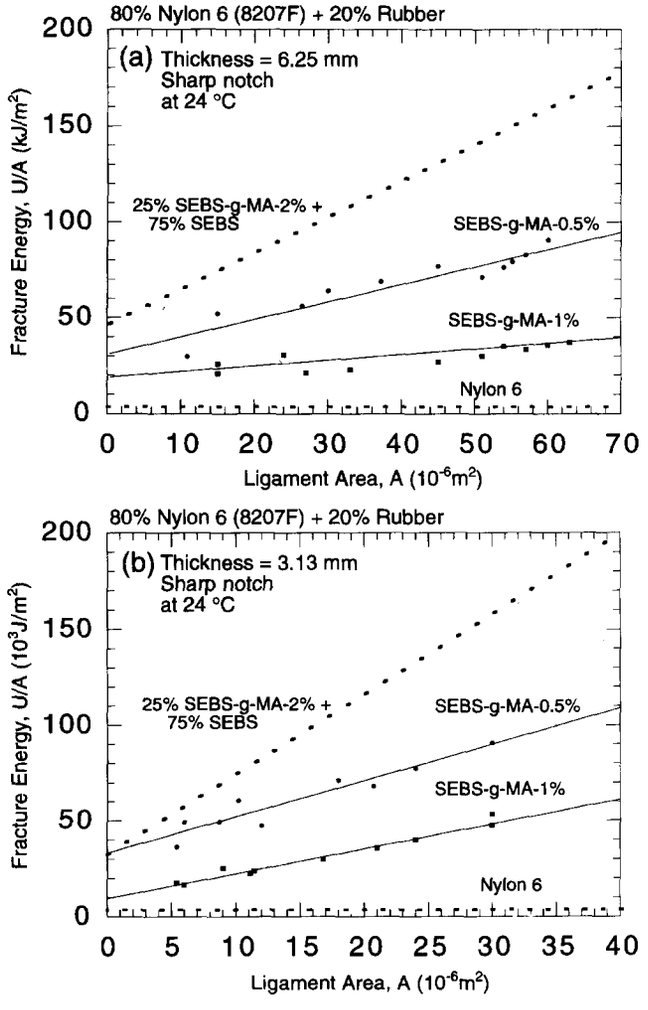

Figure 19 Fracture energy as a function of ligament area for thick specimens (a) and thin specimens (b) with sharp notches of the blends based on SEBS-*g*-MA-X% at 24°C

OBSERVATION OF REGION AROUND AN ARRESTED CRACK

In order to understand the deformation processes that occur in these rubber toughened nylon 6 blends, cracks formed during high speed testing of 6.25 mm thick specimens with sharp notches were arrested, and the

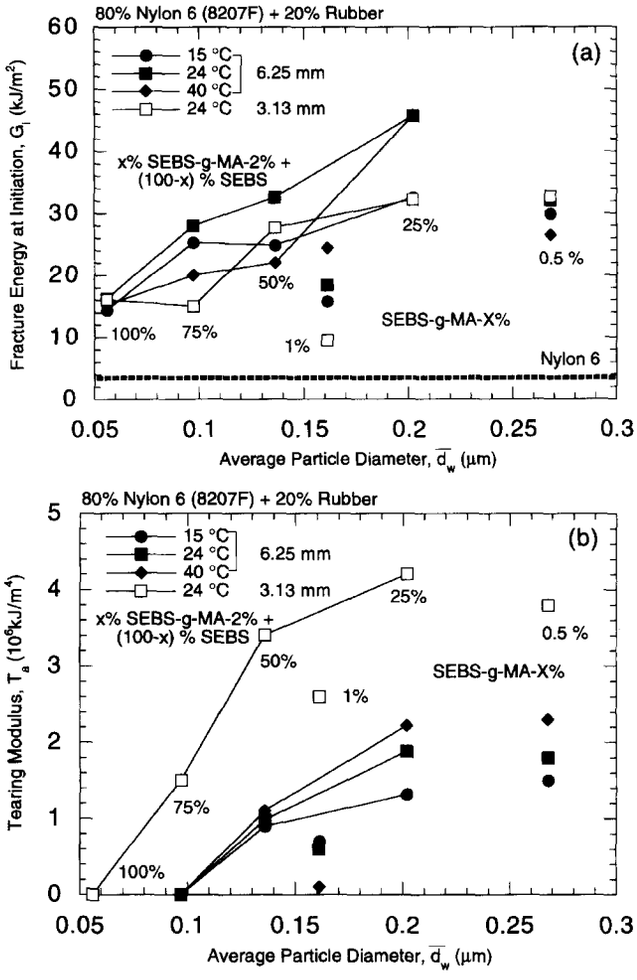

Figure 20 Fracture energy at initiation (a) and tearing modulus (b) as a function of average rubber particle diameter

surrounding region was examined by TEM using the techniques described earlier.

Figure 21 contains composites of several photomicrographs that show the regions near and well forward of the arrested crack tip or path for various blends based on SEBS-*g*-MA-2%/SEBS mixtures. These observations reveal three roughly separate regions: a zone of extensive shear yielding, a zone of shear yielding, and a zone where rubber particles cavitate. The crack tips show branching and/or blunting behaviour in these blends; crack opening distance becomes larger as the blend contains less SEBS-*g*-MA-2%, i.e. blends with larger rubber particles.

Figure 22 is a high magnification TEM photomicrograph from the cavitation zone of the blend containing 100% SEBS-*g*-MA-2% in the rubber phase; the location is identified in *Figure 21a*. There are a number of very small white spots in the region at the border between the shear yield zone and the apparent non-deformed zone. Dark field conditions do not provide definitive evidence for the presence of cavities in the rubber particles; however, there may be some cavitation in these very small rubber particles, as explained later. TEM photomicrographs from the cavitation zone for the blend based on the 25% SEBS-*g*-MA-2% + 75% SEBS mixture under bright field (*Figure 23a*) and dark field (*Figure 23b*) conditions do give evidence of holes in the rubber particles; however, all white spots under bright

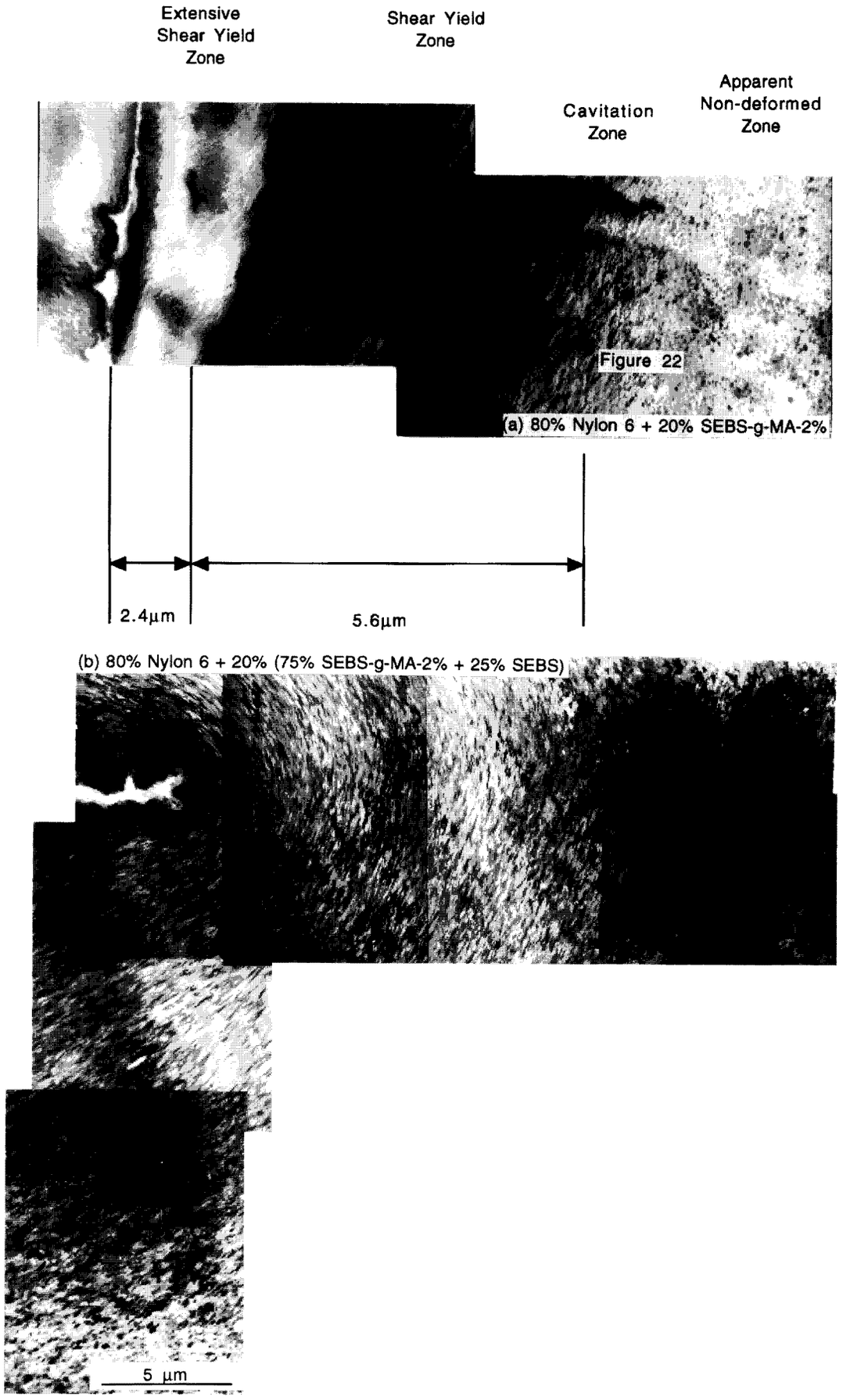

Figure 21 TEM photomicrographs showing the morphology of the deformed zone in the vicinity of the arrested crack tip for the blends based on: (a) 100% SEBS-*g*-MA-2%; (b) 75% SEBS-*g*-MA-2% and 25% SEBS; (c) 50% SEBS-*g*-MA-2% and 50% SEBS; (d) 25% SEBS-*g*-MA-2% and 75% SEBS

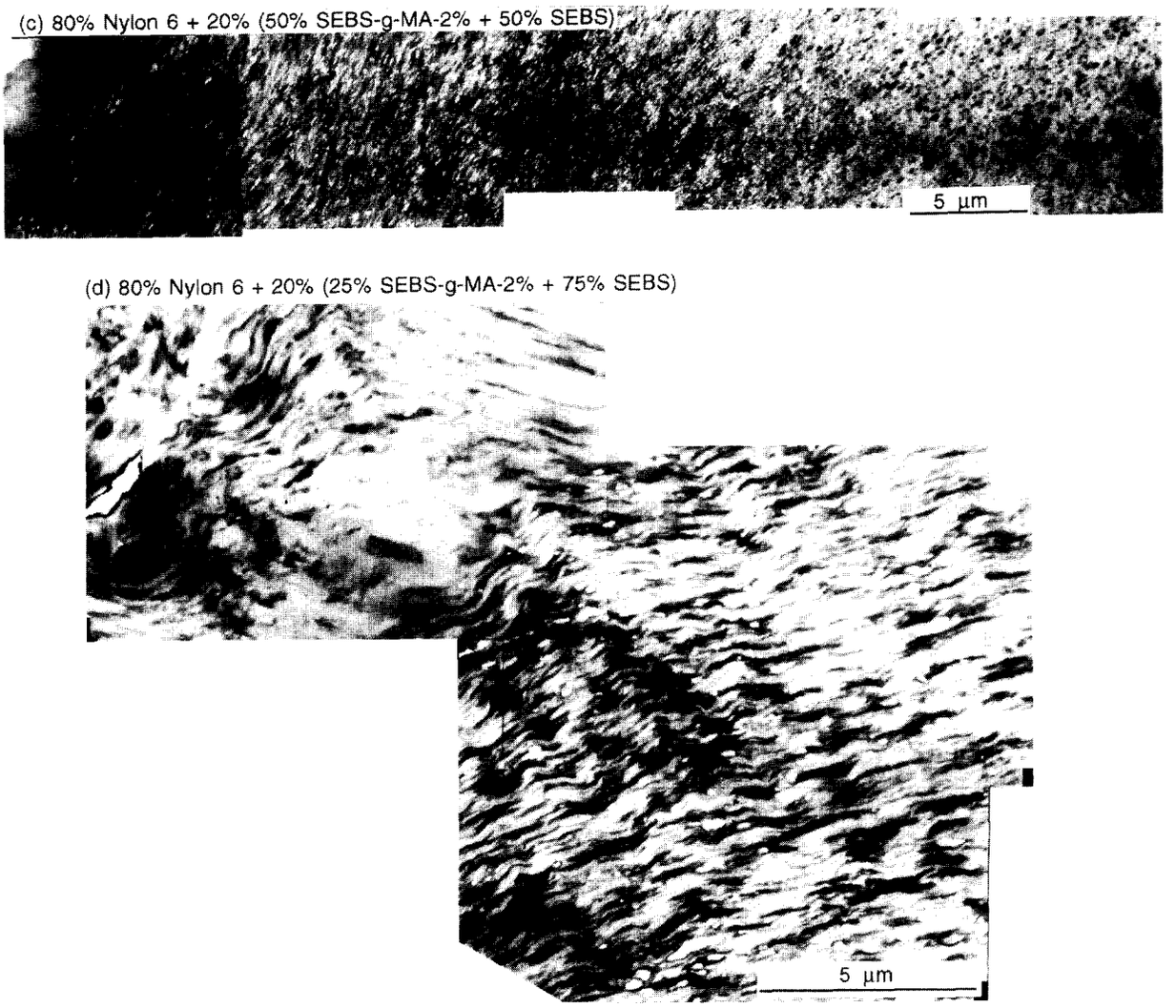

Figure 21 (*Continued*)

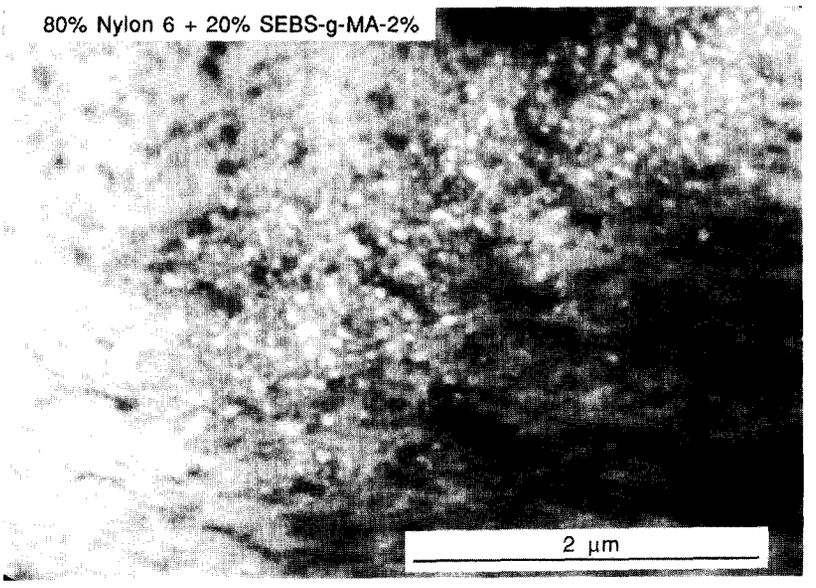

Figure 22 TEM photomicrograph under bright field conditions for a blend based on 100% SEBS-g-MA-2% in the region ahead of crack tip where particle cavitation occurs

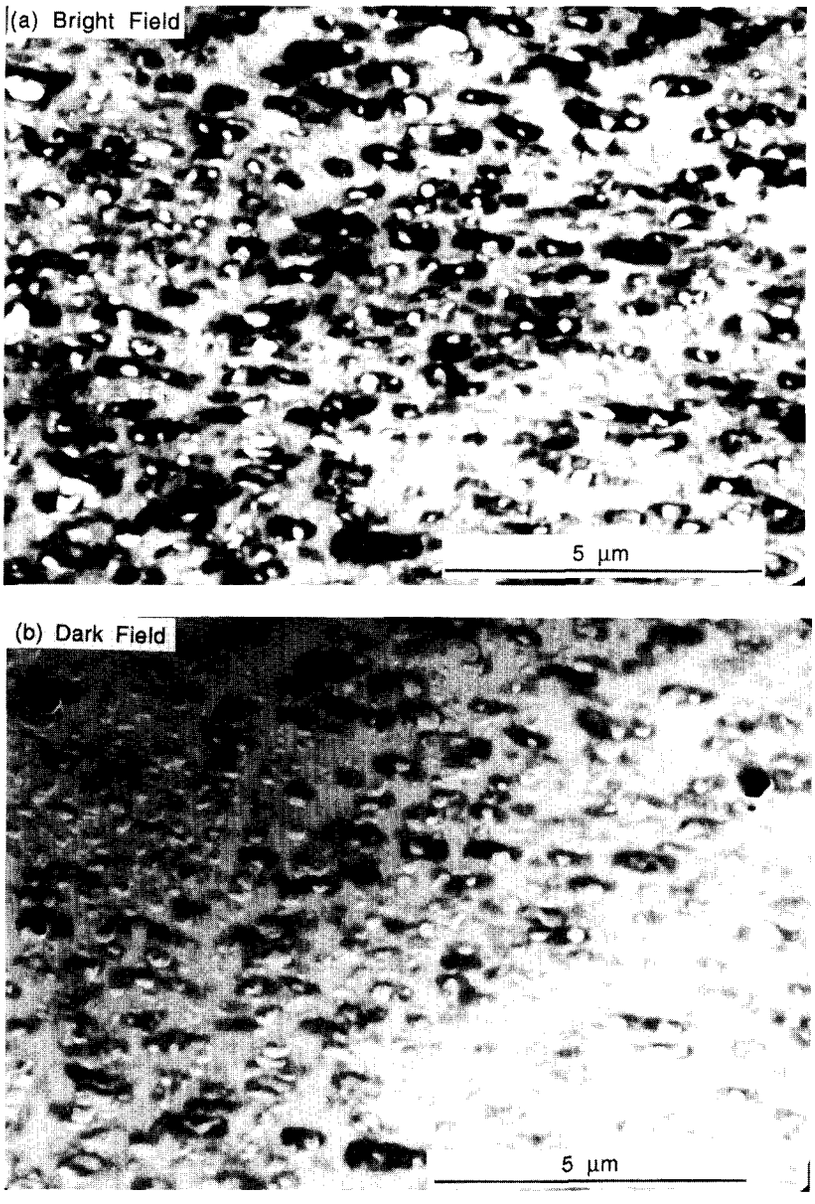

Figure 23 TEM photomicrographs under bright field (a) and dark field (b) conditions for a blend based on 25% SEBS-*g*-MA-2% and 75% SEBS

field conditions do not appear as a black spots under dark field conditions. A potential explanation of this is suggested in *Figure 24*. The microtomed sections are thin, 15–20 nm, compared to the diameter of the rubber particles in the blend based on the SEBS-*g*-MA-2% material, typically 50 nm (*Figure 24a*). Thus, the microtome cut may transverse a cavity that does not go all the way through the section. In the bright field these particles will show lighter regions than particles without cavities, but will not necessarily appear as black spots in the dark field. On the other hand, microtomed slices of blends with larger rubber particles, like the blend based on a 25% SEBS-*g*-MA-2% + 75% SEBS mixture, which has an average particle size of about 150 nm, should show more holes than blends with smaller rubber particles (*Figure 24b*). In any case, the black spots in the dark field represent definitive evidence of cavitation in some of the particles, while the above interpretation of the bright field views suggests that cavitation is even more extensive than shown in dark field. Nylon 6 blends based on SEBS-*g*-MA materials do not show post-yield volume changes during slow speed uniaxial extension which can be considered as evidence that rubber cavitation does not occur; however, nylon 6 blends based on EPR-*g*-MA, clearly do cavitate in this situation[56]. SEBS-*g*-MA particles in a nylon 6 matrix show cavitation under triaxial stress conditions near crack tips during impact loading[56]. SEBS type rubber apparently requires more severe stress conditions to cavitate compared to the blends based on EPR type rubber. The size of the deformed zone, *a*, as shown schematically in *Figure 25a* was determined using composites of several TEM photomicrographs. Values of the thickness, *a*, varied from 8 to 75 μm. This is much smaller than the size of the whitened zone defined in *Figure 25b*, which ranges from 0.1 to 1.8 mm; however, there is a definite correlation between the size of the visually observed whitened zone and the size of the deformed zone seen in TEM photomicrographs (see *Table 3*). For nylon 6 blends with SEBS-*g*-MA-2%/SEBS mixtures, both the deformed zone seen by TEM and the whitened zone seen visually (*Figure 26*) increase in size the lower the amount of SEBS-*g*-MA-2% in the rubber phase or the larger the rubber particles.

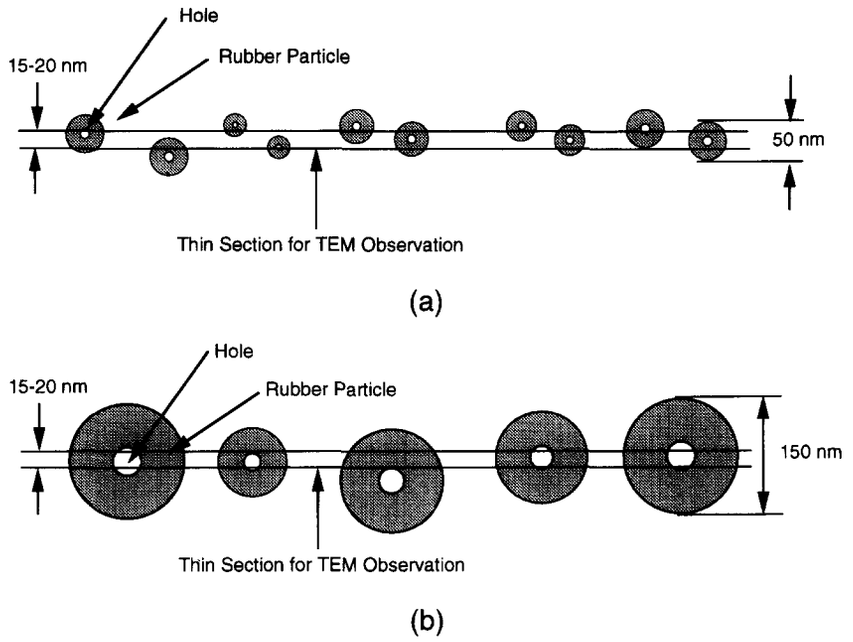

Figure 24 Schematic showing the microtomed section cut from the cavitated region of blends with small (a) and large (b) rubber particles compared to the section thickness for TEM observation

Figure 27a shows the relationship between the deformed zone size, a, and the weight-average rubber particle size, $\bar{d}_w$. Blends based on both SEBS-*g*-MA-2%/SEBS mixtures and the SEBS-*g*-MA-X% series of rubber show well-defined linear relationships; however, the latter has a lower slope. For the same rubber particle size, blends based on SEBS-*g*-MA-2%/SEBS mixtures show larger TEM deformed zones and are tougher at room temperature than those based on SEBS-*g*-MA-X% materials. As mentioned earlier, blends based on SEBS-*g*-MA-X% materials tend to have a narrower distribution of particle sizes and larger interparticle distances than blends based on SEBS-*g*-MA-2%/SEBS mixtures. The Dynatup impact strength at room temperature for thick specimens with sharp notches shows a strong, unique correlation with the size of the deformed zone size, a, for all blends considered here (*Figure 27b*). This result suggests that the main mechanism of energy absorption is plastic deformation of the nylon 6 matrix and impact energy absorption per unit volume essentially does not change by addition of rubber. The addition of rubber simply increases the size of the deformed zone.

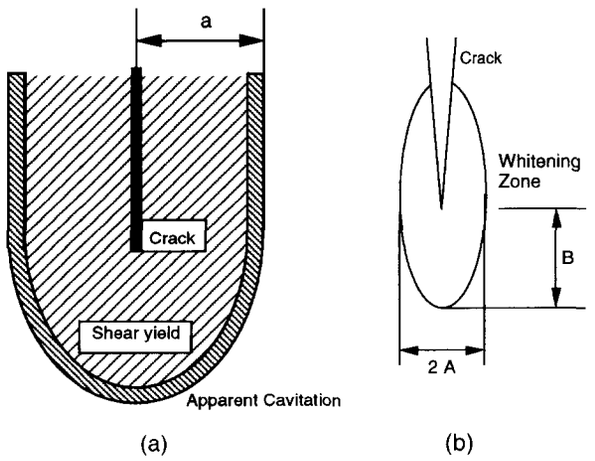

Figure 25 Schematic showing: (a) the deformed zone under TEM; (b) the whitened zone in the vicinity of the arrested crack tip

RELATIONSHIP BETWEEN DEFORMATION ZONE SIZE AND THE VU-KHANH FRACTURE PARAMETERS

The Vu-Khanh fracture parameters, G_i and T_a, are shown as functions of the deformed zone size obtained by TEM in *Figure 28*. The relationship between the fracture energy at initiation and deformed zone size (*Figure 28a*) suggests that G_i consists of two different components: energy absorption by yielding, which increases with deformed zone size, and the energy associated with elastic processes, e.g. surface energy of crack formation and possibly other mechanisms. *Figure 28b* shows that the tearing modulus is zero until the deformed zone is larger than a certain critical value, after which there is a linear relationship between the tearing modulus and the size of the deformed zone. There is a different critical deformed zone size for the SEBS-*g*-MA-X% series than for those based on mixtures of maleated and non-maleated rubber. Since both G_i and T_a appear to be related to the size

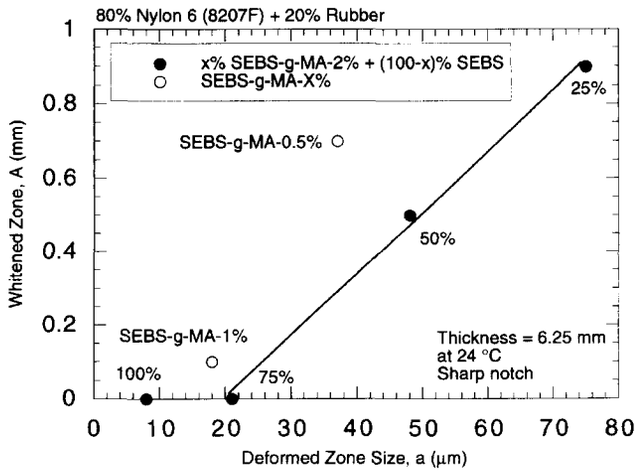

Figure 26 Whitened zone size, A as a function of deformed zone size, a, for thick specimens with sharp notch at 24°C

of the deformed zone, it is clear that at least for this series of blends that these two parameters are not fully independent of each other. This is shown by the strong correlation between G_i and T_a seen in *Figure 29*. It should be pointed out that addition of rubber in a sub-optimal manner does increase G_i while T_a remains zero; however, beyond a certain point further improvements in G_i seems to lead to increased values of T_a as well. It is not yet clear how effectively the two parameters can be varied independently by formulation.

SUMMARY AND CONCLUSIONS

The fracture characteristics of nylon 6 blends containing 20% maleated SEBS elastomers have been characterized by a variety of techniques. The degree of maleation of the rubber phase was varied by the amount of MA grafted to each elastomer molecule, SEBS-*g*-MA-X% series, or by mixing a maleated and an unmaleated elastomer, SEBS-*g*-MA-2% + SEBS series. The average rubber particle size decreases as the amount of MA in the rubber phase increases; all rubber particles in these experiments were at the low end of the particle size range for optimum toughening. Thus, for both series of elastomers, all measures of toughness increased as the average rubber particle size increased. For a fixed average rubber particle size, the SEBS-*g*-MA-2% + SEBS series lead to higher

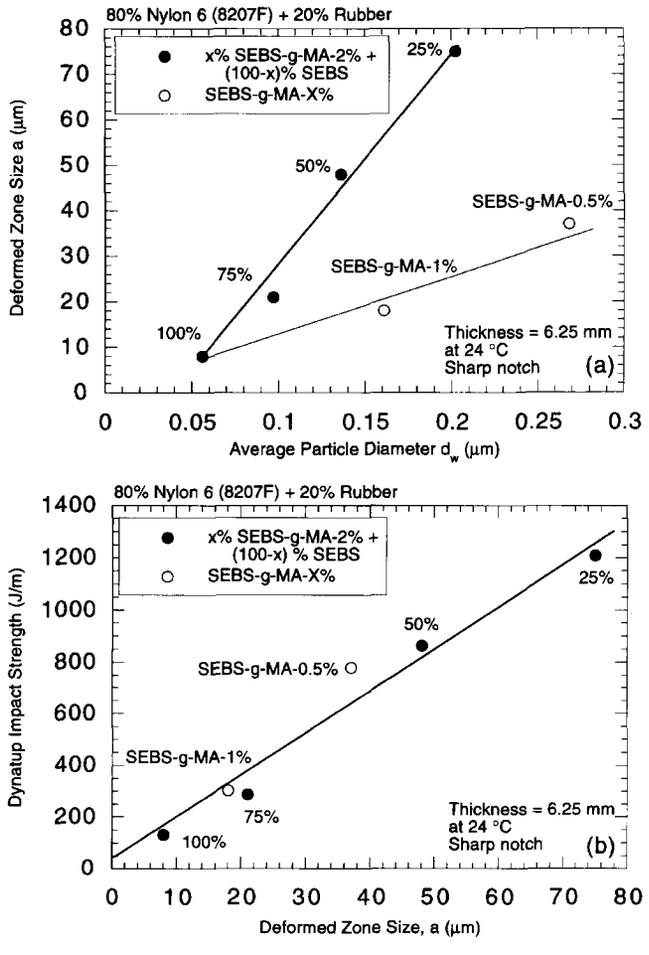

Figure 27 Deformed zone size, *a*, as a function of average rubber particle size (a) and Dynatup impact strength as a function of deformed zone size, *a* (b) from TEM observation of thick specimens with sharp notches at 24°C

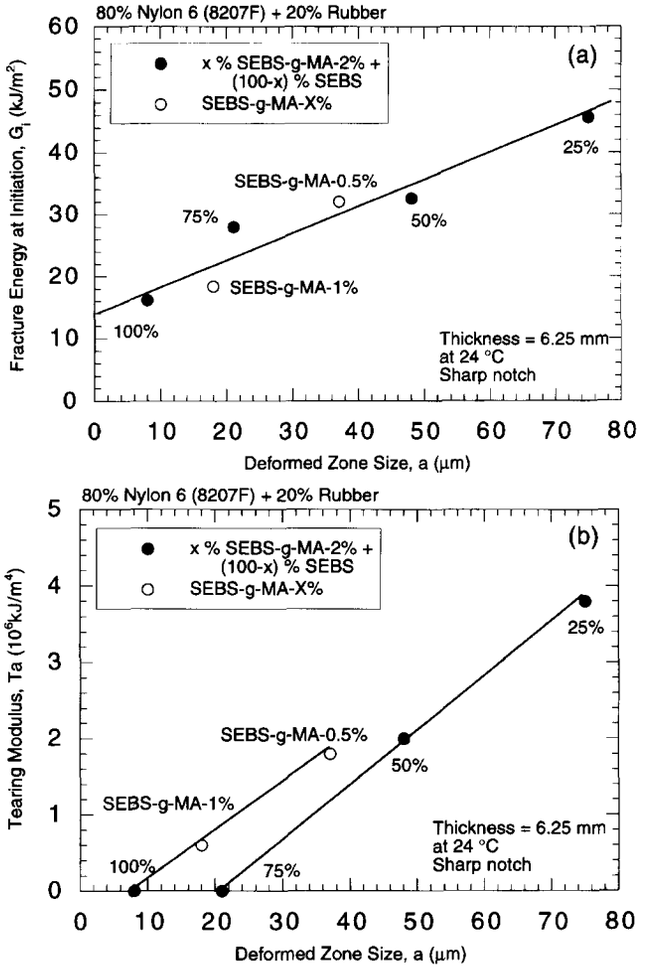

Figure 28 Fracture energy at initiation (a) and tearing modulus (b) as a function of deformed zone size, *a*, for thick specimens with sharp notches at 24°C

levels of toughness regardless of the method of evaluation. The fracture energy at initiation and tearing modulus (as determined by the Vu-Khanh methodology) plus the size of the deformed zone (as determined by TEM analysis) increase as the rubber particles become larger; however, the relationships for the two rubber series are different. However, the fracture energy seems to be uniquely related

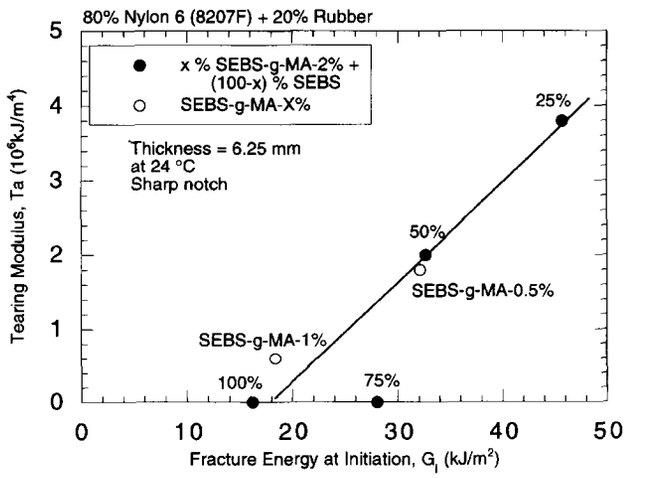

Figure 29 Tearing modulus as a function of fracture energy at initiation for thick specimens with sharp notches at 24°C

to the size of the deformed zone. Thus, it seems that predicting the size of this zone is the key to understanding toughening of such blends. The onset of super-tough behaviour appears to be related to the emergence of finite values of the tearing modulus. Such materials show ductile fracture under plain strain conditions caused by either thick specimens or sharp notches. Toughening is caused by shear yielding of the nylon 6 matrix which is evidently triggered by rubber particle cavitation. Blends containing very small rubber particles (*ca* 50 nm) are not tough, and such particles show very little cavitation during fracture.

ACKNOWLEDGEMENTS

This research was supported by the US Army Research Office and Mitsubishi Gas Chemical Co. The authors express their appreciation to Allied-Signal Inc. and Shell Development Co. for their assistance with the various materials used.

REFERENCES

1 Lawson, D. F., Hergenrother, W. L. and Matlock, M. G. *J. Appl. Polym. Sci.* 1990, **39**, 2331
2 Gilmore, D. W. and Modic, M. J. *Plastics Eng.* 1989, **45** (April), 29
3 Wu, S. *J. Appl. Polym. Sci.* 1988, **35**, 549
4 Borggreve, R. J. M., Gaymans, R. J. and Eichenwald, H. M. *Polymer* 1989, **30**, 78
5 Hobbs, S. Y., Bopp, R. C. and Watkins, V. H. *Polym. Eng. Sci.* 1983, **23**, 380
6 Borggreve, R. J. M., Gaymans, R. J., Schuijer, J. and Ingen Housz, J. F. *Polymer* 1987, **28**, 1489
7 Epstein, B. N. US Patent 4174358 (to DuPont), 1989
8 Wu, S. *Polym. Eng. Sci.* 1987, **27**, 335
9 Borggreve, R. J. M. and Gaymans, R. J. *Polymer* 1989, **30**, 63
10 Borggreve, R. J. M., Gaymans, R. J. and Schuijer, J. *Polymer* 1989, **30**, 71
11 Oshinski, A. J., Keskkula, H. and Paul, D. R. *Polymer* 1992, **33**, 268
12 Oshinski, A. J. Keskkula, H. and Paul, D. R. *Polymer* 1992, **33**, 284
13 Fayt, R., Jerome, R. and Teyssie, R. *ACS Symp. Ser.* 1989, **395**, 38
14 Lambla, M., Yu, R. X. and Lorek, S. *ACS Symp. Ser.* 1989, **385**, 67
15 Cimmino, S., Coppola, F., D'Orazio, L., Greco, R., Maglio, G., Malianconico, M., Mancerella, C., Martuscelli, E. and Ragosta, G. *Polymer* 1986, **27**, 1874
16 Bucknall, C. B. 'Toughened Plastics', Applied Science, London, 1977
17 Boyer, R. F. and Keskkula, H. in 'Encyclopedia of Polymer Science and Technology' (Eds H. F. Mark, N. G. Gaylord and N. M. Bikales), Vol. 13, Wiley, New York, 1970, p. 375
18 Turley, S. G. and Keskkula, H. *Polymer* 1980, **21**, 466
19 Donald, A. M. and Kramer, E. J. *Polymer* 1985, **26**, 1855
20 Keskkula, H. 'Adv. Chem. Ser. 222' (Ed. Riew, C. K.), Amer. Chem. Soc., Washington, DC, 1989, p. 289
21 Wu, S. *J. Appl. Polym. Sci.* 1988, **35**, 549
22 Bucknall, C. B., Heather, P. S. and Lazzeri, A. *J. Mater. Sci.* 1989, **16**, 2255
23 Bucknall, C. B., Karpodinis, A. and Zhan, X. C. *J. Mater. Sci.* 1994, **29**, 3377
24 Partridge, I., Sanz, C. and Bickerstaff, K. 'Proceedings of The 5th Annual Meeting of the Polymer Processing Society', Tokyo, Japan, 1989, p. 218
25 Bernstein, H. L. in 'Elastic-Plastic Test Methods: The User's Experience (Second Volume), ASTM STP 1114' (Ed. J. A. Joyce), ASTM, Philadelphia, 1991, p. 306
26 Chung, W. N. and Williams, J. G. in 'Elastic-Plastic Test Methods: The User's Experience (Second Volume), ASTM STP 1114' (Ed. J. A. Joyce), ASTM, Philadelphia, 1991, p. 320
27 Crouch, B. A. and Huang, D. D. *J. Mater. Sci.* 1994, **29**, 861
28 Duffy, J. and Shih, C. F. 'Advances in Fracture Research. Proceedings of the 7th International Conference on Fracture (ICF7)', 1989, p. 633
29 Hashemi, S. and Williams, J. G. *J. Mater. Sci.* 1991, **26**, 621
30 Huang, D. D. in 'Elastic-Plastic Test Methods: The User's Experience (Second Volume), ASTM STP 1114' (Ed. J. A. Joyce), ASTM, Philadelphia, 1991, p. 290
31 Mai, Y. -W. and Powell, P. *J. Polym. Sci., Part B: Polym. Phys.* 1991, **29**, 785
32 Takemori, M. T. and Narisawa, I. 'Advances in Fracture Research. Proceedings of the 7th International Conference on Fracture (ICF7)', 1989, p. 2733
33 Vu-Khanh, T. *Polymer* 1988, **29**, 1979
34 Wu, J. and Mai, Y.-W. *J. Mater. Sci.* 1993, **28**, 6167
35 Vu-Khanh, T. and De Charentenay, F. X. *Polym. Eng. Sci.* 1985, **25**, 841
36 Paton, C. A. and Hashemi, S. *J. Mater. Sci.* 1992, **27**, 2279
37 Zhou, Z., Landes, J. D. and Huang, D. D. *Polym. Eng. Sci.* 1994, **34**, 128
38 Huang, D. D. and Williams, J. G. *J. Mater. Sci.* 1987, **22**, 2503
39 Huang, D. D. *Soc. Plast. Eng., ANTEC 1991*, **49**, 582
40 Seidler, S. and Grellmann, W. *J. Mater. Sci.* 1993, **28**, 4078
41 'E-399 Standard Test Method for Plane-Strain Fracture Toughness of Metallic Materials', Annual Book of ASTM standards, American Society for Testing and Materials, Philadelphia, 1990
42 Williams, J. G. 'Fracture Mechanics of Polymers', Ellis Horwood, Chichester, 1984
43 'E-813 Standard Test Method for J_{1c}, A measure of Fracture Toughness, Annual Book of ASTM standards, American Society for Testing and Materials, Philadelphia, 1989
44 Mai, Y.-W. *Polym. Commun.* 1989, **30**, 330
45 Mai, Y. W. and Cotterell, B. *Int. J. Fracture* 1986, **32**, 105
46 Mai, Y.-W., Cotterell, B., Horlck, R. and Vigna, G. *Polym. Eng. Sci.* 1987, **27**, 804
47 Hodgkinson, J. M. and Williams, J. G. *J. Mater. Sci.* 1981, **16**, 50
48 Chung, I., Throckmorton, E. and Chundury, D. *Soc. Plast. Eng., ANTEC 1979*, **37**, 681
49 Pai, Chih-Chiang Jeng, Ru-Jong Grossman, Steven J. and Huang, Jan-Chan *Adv. Polym. Tech.* 1989, **2**, 157
50 Oshinski, A. J., Keskkula, H. and Paul, D. R. *Polymer* 1996, **37**, 4891
51 Oshinski, A. J., Keskkula, H. and Paul, D. R. *Polymer* 1996, **37**, 4909
52 Oshinski, A. J., Keskkula, H. and Paul, D. R. *Polymer* 1996, **37**, 4919
53 Kohan, M. I. (Ed.), 'Nylon Plastics Handbook', Hanser, Munich, 1995
54 Kayano, Y., Keskkula, H. and Paul, D. R. *Polymer* (in press)
55 Broek, D. 'Elementary Engineering Fracture Mechanics', Noordoff International Publishing, Leyden, 1974
56 Gonzalez-Montiel, A., Keskkula, H. and Paul, D. R. *Polymer* 1995, **36**, 4621